# Evaluation of lipid biomarkers as proxies for sea ice and ocean temperatures along the Antarctic continental margin

Nele Lamping[1], Juliane Müller[1,2,3], Jens Hefter[1], Gesine Mollenhauer[1,2,3], Christian Haas[1], Xiaoxu Shi[1], Maria-Elena Vorrath[1], Gerrit Lohmann[1,3,4], Claus-Dieter Hillenbrand[5]

[1]Alfred Wegener Institute, Helmholtz Center for Polar and Marine Research, Am Alten Hafen 26, 27568 Bremerhaven, Germany

[2]Department of Geosciences, University of Bremen, Klagenfurter Straße, 28359 Bremen, Germany

[3]Marum - Center for Marine Environmental Sciences, Leobener Straße 8, 28359 Bremen, Germany

[4]Department of Environmental Physics, University of Bremen, 28359 Bremen, Germany

[5]British Antarctic Survey, High Cross, Madingley Road, Cambridge CB3 0ET, United Kingdom

*Correspondence to: Nele Lamping (nele.lamping@awi.de)*

## Abstract

The importance of Antarctic sea ice and Southern Ocean warming has come into the focus of polar research ~~in~~during the last couple of decades. Especially ~~in~~around West Antarctica, where warm water masses approach the continent and where sea ice has declined, the distribution and evolution of sea ice play a critical role for the stability of nearby ice shelves. Organic geochemical analyses of marine seafloor surface sediments from the Antarctic continental margin ~~permit~~allow an evaluation of the applicability of biomarker-based sea ice and ocean temperature reconstructions in these ~~vulnerable~~climatically sensitive areas. We analysed highly branched isoprenoids (HBIs), such as the sea-ice proxy $IPSO_{25}$ and phytoplankton-derived HBI-trienes, but also phytosterols and isoprenoidal glycerol dialkyl glycerol tetraethers (GDGTs), which are established tools for the assessment of primary productivity and ocean temperatures, respectively. The combination of $IPSO_{25}$ with a phytoplankton marker (*i.e.* the $PIPSO_{25}$ index) permits semi-quantitative sea-ice reconstructions and avoids

misleading over- or underestimations of sea-ice cover. Comparisons of the PIPSO$_{25}$-based sea-ice distribution patterns and TEX$^L_{86}$- and RI-OH'-derived ocean temperatures with (1) sea-ice concentrations obtained from satellite observations and (2) ~~instrumental~~instrument measurements of sea surface and subsurface temperatures corroborate the general capability of these proxies to ~~properly display~~determine oceanic key variables properly. This is further supported by model data. We also highlight specific aspects and limitations that need to be ~~considered when interpreting~~taken into account for the interpretation of such biomarker data and discuss the potential of IPSO$_{25}$ ~~to reflect~~as an indicator for the former occurrence of platelet ice and/or the export of ice shelf water.

**1. Introduction**

2  One of the key components of the global climate system, influencing major atmospheric and oceanic

3  processes, is floating on the ocean's surface at high latitudes – sea ice (Thomas, 2017). Southern Ocean

4  sea ice is one of the most strongly changing features of the Earth's surface as it experiences considerable

5  seasonal variabilities with ~~decreasing~~ sea-ice extent decreasing from a maximum of 20 x $10^6$ $km^2$ in

6  September to a minimum of 4 x $10^6$ $km^2$ in March (Arrigo et al., 1997; Zwally, 1983). This seasonal

7  waxing and waning of sea ice substantially modifies deep-water formation ~~as well as~~, influences the

8  ocean-atmosphere exchange of heat and gas~~,~~ and strongly affects surface albedo and radiation budgets

9  (Abernathey et al., 2016; Nicholls et al., 2009; Turner et al., 2017~~, and also~~). Moreover, sea ice

10  regulates ocean buoyancy flux, upwelling and primary production (Schofield et al., 2018).

11  Based on the 40-year satellite record, Southern Ocean sea-ice extent as a whole followed an increasing

12  trend (Comiso et al., 2017; Parkinson and Cavalieri, 2012), experiencing an abrupt reversal from

13  ~~2014~~ca. 2015 to 2018 (Parkinson, 2019; Turner et al., 2020; Wang et al., 2019), which has been

14  attributed to a ~~decade~~decades-long oceanic warming and increased advection of atmospheric heat

15  (Eayrs et al., 2021). However, the sea-ice extent around major parts of West Antarctica has been

16  decreasing over the last 40 years~~.~~ (Parkinson and Cavalieri, 2012). The Antarctic Peninsula is

17  particularly affected by a significant reduction in sea-ice extent and rapid atmospheric and oceanic

18  warming (Etourneau et al., 2019; Li et al., 2014; Massom et al., 2018; Vaughan et al., 2003). The Larsen

19  ~~Ice Shelves~~ A and B~~, located~~ ice shelves on the east coast of the Antarctic Peninsula~~,~~ collapsed in 1995

20  and 2002, respectively~~, which was~~. These collapses were triggered by the loss of a sea-ice buffer,

21  ~~enabling~~which enabled an increased flexure of the ice-shelf margins by ocean ~~swells~~swell (Massom et

22  al., 2018). ~~The~~Along the Pacific margin of West Antarctica, the Bellingshausen and Amundsen ~~Seas~~

23  ~~are~~seas have also been affected by ~~a~~ major sea-ice decline and regional surface ocean warming (Hobbs

24  et al., 2016; Parkinson, 2019). Marine-terminating glaciers draining into the Amundsen ~~Sea~~and

25  Bellingshausen seas are thinning at an alarming rate, which has been linked to sub-ice shelf melting

26  caused by relatively warm Circumpolar Deep Water (CDW) incursions into sub-ice shelf cavities (*e.g.*,

27  Jacobs et al., 2011; Khazendar et al., 2016; Nakayama et al., 2018; Rignot et al., 2019; Smith et al.,

28  2017). The disintegration of ice shelves reduces the buttressing effect that they exert on ice grounded

**hat formatiert:** Englisch (Vereinigte Staaten)

29  further upstream, which ~~may~~can lead to ~~a~~ partial ~~collapse~~or total loss of the ice in the catchments of the

30  affected glaciers~~, eventually raising~~ and, thus, raise global sea level considerably (3.4 to 4.4 m ~~resulting~~

31  ~~from a WAIS~~in case of a total West Antarctic Ice Sheet collapse; Fretwell et al., 2013; Jenkins et al.,

32  2018; Pritchard et al., 2012; Vaughan, 2008).

33  State-of-the-art climate models are not yet fully able to depict sea-ice seasonality and sea-ice cover,

34  which the 5$^{th}$ Assessment Report of the Intergovernmental Panel on Climate Change (Stocker et al.,

35  2013) attributes to a lack of validation efforts using proxy-based sea-ice reconstructions. Knowledge

36  about (paleo-)sea-ice conditions and ocean temperatures in the climate sensitive areas around the West

37  Antarctic Ice Sheet is hence considered as crucial for understanding past and future climate evolution.

38  To date, the most common proxy-based sea-ice reconstructions in the Southern Ocean ~~are conducted~~

39  ~~by the use~~utilize fossil assemblages of sympagic ~~diatom assemblages, which are strongly dependent on~~

40  ~~their preservation~~(*i.e.* living within ~~the~~sea ice) diatoms preserved within the seafloor sediments (Allen

41  et al., 2011; Armand and Leventer, 2003; Crosta et al., 1998; Esper and Gersonde, 2014; Gersonde and

42  Zielinski, 2000; Leventer, 1998). Dissolution effects within the water column or after deposition,

43  however, determine the preservation ~~state~~ of ~~the~~ small, lightly silicified ~~microfossils~~diatom taxa and

44  ~~may~~therefore can alter the ~~diatom~~assemblage record, leading to inaccurate sea-ice reconstructions

45  (Leventer, 1998; Zielinski et al., 1998). Recently, the molecular remains of certain ~~diatoms,~~diatom taxa,

46  i.e. specific organic geochemical lipids, have emerged as a potential proxy for reconstructing past

47  Antarctic sea-ice cover (Barbara et al., 2013; Collins et al., 2013; Crosta et al., 2021; Denis et al., 2010;

48  Etourneau et al., 2013; Lamping et al., 2020; Massé et al., 2011; Vorrath et al., 2019; 2020).

49  Specifically, a di-unsaturated highly branched isoprenoid (HBI) alkene (HBI diene, $C_{25:2}$) has been

50  detected in both sea-ice diatoms ~~and sediments in~~from the Southern Ocean and Antarctic marine

51  sediments (Johns et al., 1999; Massé et al., 2011; Nichols et al., 1988~~), and recently~~). Recently, the

52  sympagic ~~(*i.e.* living within sea ice) tube-dwelling~~ diatom *Berkeleya adeliensis* ~~has been identified as~~

53  ~~producer~~, which preferably proliferates in platelet ice, has been identified as the producer of these HBI

54  alkene (Belt et al., 2016; Riaux-Gobin and Poulin, 2004). However, *B. adeliensis* seems rather flexible

55  concerning its habitat, since it was also recorded in the bottom ice layer and ~~seems to be~~is apparently

56  well adapted to changes in texture during ice melt (Riaux-Gobin et al., 2013). Belt et al. (2016)

2

57  introduced the term $IPSO_{25}$ ("Ice Proxy of the Southern Ocean with 25 carbon atoms") by analogy to

58  the counterpart $IP_{25}$ in the Arctic. Commonly, for a more detailed assessment of sea-ice conditions, $IP_{25}$

59  in the Arctic Ocean and $IPSO_{25}$ in the Southern Ocean have been measured alongside complementary

60  phytoplankton-derived lipids, such as sterols and/or HBI-trienes, which are indicative of open-water

61  conditions (Belt and Müller, 2013; Lamping et al., 2020; Etourneau et al., 2013; Vorrath et al., 2019;

62  2020). The combination of the sea-ice biomarker and a phytoplankton biomarker, the so-called $PIPSO_{25}$

63  index (Vorrath et al., 2019), allows for a more quantitative differentiation of contrasting sea-ice settings

64  and helps to avoid misinterpretations of the absence of $IPSO_{25}$ which. An absence of the sea-ice

65  biomarker can result from either a lack of sea-ice cover or a permanentlypermanent thick sea-ice cover,

66  that prevents light penetration and hence limitinglimits ice algae growth. These two contrasting

67  scenarios can be distinguished by using the additional phytoplankton biomarker. Recently, Lamping et

68  al. (2020) used this approachthe $PIPSO_{25}$ index to studyreconstruct changes in sea-ice conditions during

69  the last deglaciation of the Amundsen Sea shelf, which were likely linked to advance and retreat phases

70  of the Getz Ice Shelf.

71  Multiple mechanisms exist that can cause ice-shelf instability. As previously mentioned, relatively

72  warm CDW is considered one of the main drivers for ice-shelf thinning in the Amundsen Sea

73  Embaymentand Bellingshausen Sea sectors of the West Antarctic Ice Sheet (Nakayama et al., 2018;

74  Jenkins and Jacobs, 2008; Rignot et al., 2019). Accordingly, changing ocean temperatures are another

75  crucial factor for the stability of the marine-based ice streams draining most of the West Antarctic Ice

76  Sheet (e.g., Colleoni et al., 2018). As for sea-ice reconstructions, organic geochemical lipidslipid

77  proxies have been employed over the past decades for reconstructing ocean temperatures in high

78  latitudes have come into focus in the past decades, since the abundance and preservation of calcareous

79  microfossils, which are commonly used for such reconstructions, is very poor in polar marine sediments

80  (e.g., Zamelczyk et al., 2012). ArchaealIn contrast, archaeal isoprenoidal glycerol dialkyl glycerol

81  tetraethers (isoGDGTs), sensitive to temperature change and relatively resistant to degradation

82  processes, are well-preserved in all types of marine sediments (Huguet et al., 2008; Schouten et al.,

83  2013). Schouten et al. (2002) found that the number of rings in sedimentary GDGTs is correlated with

84    surface water temperatures and developed the first archaeal lipid paleothermometer $TEX_{86}$, a ratio of

85    certain GDGTs, as a sea surface temperature (SST) proxy. For polar oceans, Kim et al. (2010) developed

86    a more specific calibration model for temperatures below 15 °C, $TEX^{L}_{86,}$ which employs a different

87    GDGT combination. There is an emerging consensus that GDGTs ~~are rather reflecting~~predominantly

88    reflect subsurface ocean temperatures (SOT) along the Antarctic margin (Kim et al., 2012; Etourneau

89    et al., 2019; Liu et al., 2020). This is supported by observations of elevated archaeal abundances (and

90    GDGTs) in warmer subsurface waters (Liu et al., 2020; Spencer-Jones et al., 2021). Archaea adapt their

91    membrane in cold waters by adding hydroxyl groups and changing the number of rings, OH-GDGTs

92    (Fietz et al., 2020). Huguet et al. ~~The~~(2017) found in molecular dynamic simulations that the additional

93    hydroxyl moieties lead to an increase of the membrane fluidity ~~that~~, which aids trans-membrane

94    transport in cold environments~~, which~~. This explains~~Huguet et al. (2017) found in molecular dynamic~~

95    ~~simulations, explaining~~ the higher relative abundance of OH Archaea lipids in cold environments.

96    Taking the OH-GDGTs into account, Lü et al. (2015) proposed an SST-proxy for the polar oceans, the

97    RI-OH'.

98    ~~Our~~The aim ~~with this~~of our study is to provide insight into the application of biomarkers ~~for sea ice as~~

99    ~~well as ocean temperature reconstructions~~ in Southern Ocean sediments as sea ice and ocean

100   temperature proxies. Estimates on recent sea-ice coverage and ocean temperatures along the eastern and

101   western Antarctic Peninsula (EAP and WAP) as well as in the Amundsen and Weddell ~~Seas,~~seas are

102   based on the analyses of $IPSO_{25}$, HBI-trienes and phytosterols ~~as well as~~and GDGTs in seafloor surface

103   sediment samples from these areas. ~~An intercomparison~~A comparison of biomarker-~~based~~ derived

104   estimates of sea--ice ~~as well as~~extent and ocean temperature ~~estimates~~ with (1) sea-ice distributions

105   obtained from satellite observations and (2) ~~ocean temperatures deduced from instrumental data~~in-situ

106   ocean temperature measurements allows for an evaluation of the proxy ~~approaches~~approach. We further

107   consider AWI-ESM2 climate model data to assess the model's performance in depicting recent oceanic

108   key variables and to examine the potential impact of paleoclimate conditions on the biomarker

109   composition of the investigated surface sediments. ~~In regard of~~Taking into account the various factors

110   affecting the use of marine biomarkers as paleoenvironmental proxies, we ~~further~~comment on the

111   limitations of GDGT temperature estimates and the novel $PIPSO_{25}$ approach~~, and~~. Furthermore, we

4

discuss the potential connection between IPSO$_{25}$ and platelet ice formation under near-coastal fast ice, which is related to the near-surface presence of sub-ice shelf melt water.

## 2. Regional setting

The areas ~~of investigation~~investigated in this study include the southern Drake Passage, the continental shelves of the WAP and EAP (~60° S) and the more southerly located Amundsen and Weddell ~~Seas~~seas (~75° S; Fig. 1). The different study areas are all connected by the Antarctic Circumpolar Current (ACC), the Antarctic Coastal Current and the Weddell Gyre, respectively (Meredith et al., 2011; Rintoul et al., 2001).
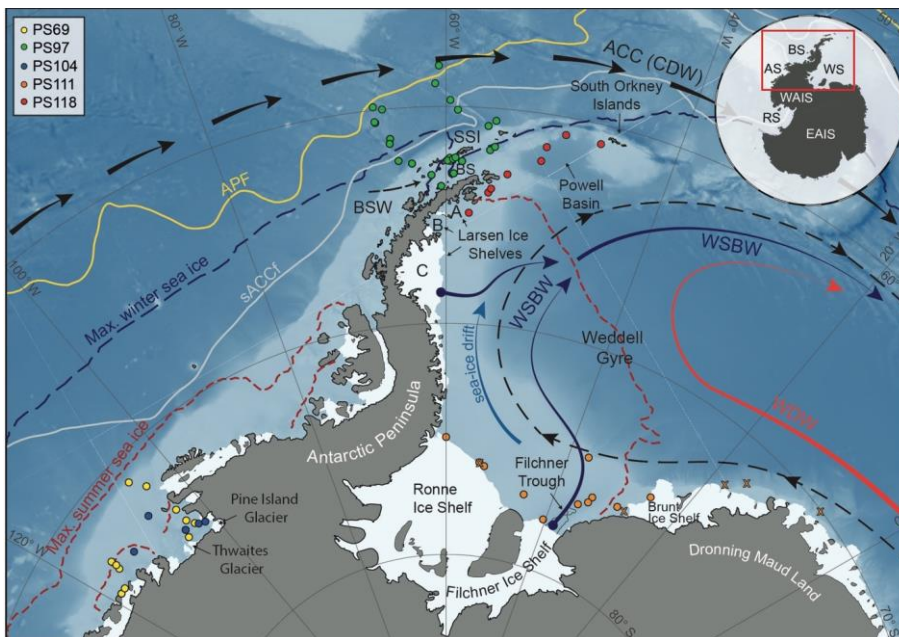


**Fig. 1:** Map of the study area (location indicated by red box in insert map) including all 41 sample locations (see different colored dots for individual RV *Polarstern* expeditions in the top left corner; for detailed sample information, see Table S1) and main oceanographic features. Maximum summer and winter sea-ice boundaries are marked by dashed red and blue line, respectively (Fetterer et al., 2016). ~~Orange~~The orange crosses in the Weddell Sea indicate samples ~~where a PIPSO$_{25}$ value of 1 has been assigned due to~~with low biomarker concentrations~~,~~ close to detection limit, to which we assigned a PIPSO$_{25}$ value of 1. ACC: Antarctic Circumpolar Current, APF: Antarctic Polar Front, sACCf: southern Antarctic Circumpolar Current Front, SSI: South Shetland Islands, BS: Bransfield Strait, BSW: Bellingshausen Sea Water, CDW: Circumpolar Deep Water; WDW: Weddell Deep Water, WSBW: Weddell Sea Bottom Water (Mathiot et al., 2011; Orsi et al., 1995). Insert map shows grounded ice ~~only (i.e., no.~~ without ice shelves~~).~~) in black; WAIS: West Antarctic Ice Sheet, EAIS: East Antarctic Ice Sheet, RS: Ross Sea, AS: Amundsen Sea, BS: Bellingshausen Sea, WS: Weddell Sea. Background bathymetry derived from IBCSO data (Arndt et al., 2013).

The ACC, which is mainly composed of CDW and characterised by strong eastward flow, is the largest current system in the world ~~characterised by a strong eastward flow, which finds~~and has its narrowest constriction in the Drake Passage. ~~Along~~In the Bellingshausen Sea, the Amundsen Sea and along the WAP, where the ACC flows close to the continental shelf edge, CDW is upwelling onto the shelf and flows to the coast via bathymetric troughs, contributing to basal melt and retreat of marine-terminating glaciers and ice shelves (Cook et al., 2016; Jacobs et al., 2011; Jenkins and Jacobs, 2008; Klinck et al., 2004). In the Weddell Sea, the Weddell Gyre, a subpolar cyclonic circulation ~~is present~~south of the ACC, ~~the Weddell Gyre, which~~ deflects part of the ACC's CDW towards the south ~~turning~~and turns it into Warm Deep Water (WDW; Fig. 1; Hellmer et al., 2016; Vernet et al., 2019). In close vicinity to the Filchner-Ronne and Larsen Ice Shelves, ~~glacially derived freshwater~~glacial meltwater as well as dense ~~brine~~brines released during sea-ice formation contribute to the formation of Weddell Sea Bottom Water (WSBW) - a major precursor of Antarctic Bottom Water (Hellmer et al., 2016). ~~Wind~~Along the EAP coast wind and currents force a northward ~~sea ice~~ drift ~~in the western Weddell Sea along the eastern coast of the Antarctic Peninsula~~sea ice (Harms et al., 2001~~) until leaving it to melt in~~), which melts when reaching warmer waters ~~to~~in the North and ~~up to the~~in Powell Basin (Vernet et al., 2019). At the northern tip of the Antarctic Peninsula, colder and saltier Weddell Sea water masses branch off westwards into the Bransfield Strait, where they encounter the well-stratified, warm, and fresh Bellingshausen Sea Water (BSW; Fig. 1), which is entering the Bransfield Strait from the West (Sangrà et al., 2011).

140 Since 1978, satellite observations show strong seasonal ~~as well as~~and decadal changes in sea-ice cover

141 ~~at the~~aroundthe Antarctic Peninsula, which are less pronounced in the ~~more southerly~~ Amundsen and

142 Weddell ~~Seas (Fig. 2a-c).~~seas (Vaughan et al., 2003; Parkinson and Cavalieri, 2012). Mean monthly

143 sea-ice concentrations (SIC) for austral winter (JJA), spring (SON) and summer (DJF) reveal a

144 permanently ice-free Drake Passage, while the WAP and EAP shelf areas are influenced by a changing

145 sea-ice cover ~~in~~throughout the ~~course of a~~ year (Fig. 2a-c). For the Amundsen and Weddell ~~Seas~~seas,

146 satellite data reveal ~~a closed seasonal sea-ice cover with~~ up to ~90 % sea-ice concentration during winter

147 and spring (Fig. 2a+b), and ~~a late break up of sea-ice cover to~~ a minimum concentration of ~30 %
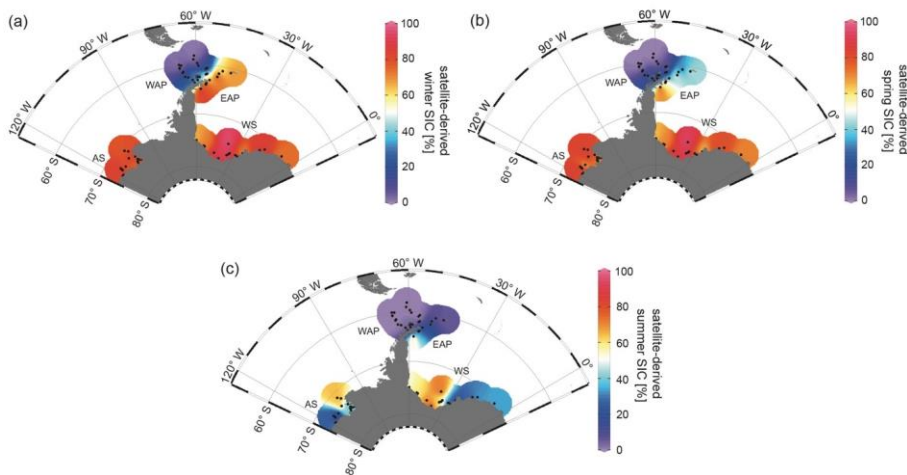
148 during summer (Fig. 2c).



**Fig. 2:** Distribution of mean monthly satellite-derived sea-ice concentrations for (a) winter (JJA), (b) spring (SON) and (c) summer (DJF) in % (downloaded from the National Snow and Ice Data Center, NSIDC; Cavalieri et al., 1996). AS: Amundsen Sea, WAP: West Antarctic Peninsula, EAP: East Antarctic Peninsula, WS: Weddell Sea.

149 **3.   Material and methods**

150    3.1   Sediment samples

151 ~~In total, we~~We analysed a set of 41 surface sediment samples (0-1 cm subbottom depth) from different

152 areas of the Southern Ocean (Fig. 1) retrieved by multicorers and giant box corers during RV *Polarstern*

153 expeditions over the past 15 years. Sixteen surface sediment samples from the Amundsen Sea

154 continental shelf were collected during ~~RV Polarstern~~ expeditions PS69 in 2006 (Gohl, 2007) and

7

155 PS104 in 2017 (Gohl, 2017). Twenty-five surface sediment samples from the southeastern and

156 southwestern Weddell Sea continental shelf were collected during *RV Polarstern* expeditions PS111 in

157 2018 (Schröder, 2018) and PS118 in 2019 (Dorschel, 2019). This new data set of samples was

158 complemented by data from 26 surface sediment samples from thecollected in Bransfield Strait/WAP

159 for, which the analytical results had been previously published by Vorrath et al. (2019).

160

161       3.2    Bulk sediment and organic geochemical analyses

162 The sediment material was freeze-dried and homogenized with an agate mortar and stored in glass vials

163 at -20 °C before and after these initial preparation steps to avoid degradation of targeted molecular

164 components. Total organic carbon (TOC) contents were measured on 0.1 g of sediment after removing

165 inorganic carbon (total inorganic carbon, carbonates) with 500 µl 12 N hydrochloric acid.

166 MeasurementsTOC contents were conducted by means of determined with a carbon-sulphur

167 determinatoranalyzer (CS 2000; Eltra) with standards being measured for calibration being routinely

168 measured before sample analysesanalysis and after every tenth sample to ensure accuracy (error ±

169 0.02 %).

170 Lipid biomarkers were extracted from the sediments (4 g for PS69 and PS104; 6 g for PS111 and PS118)

171 by ultrasonication (3 x 15 min),) using dichloromethane:methanol (3 x 6 ml for PS69 and PS104; 3 x 8

172 ml for PS111 and PS118; 2:1 v/v) as solvent. Prior to this step, the internal standards 7-hexylnonadecane

173 (7-HND; 0.038 µg/sample for PS69 and PS104 and 0.057 µg/sample for PS111 and PS118), 5α-

174 androstan-3-ol (1.04 µg/sample) and $C_{46}$ (0.98 µg/sample) were added to the sample for quantification

175 of HBIs, sterols and GDGTs, respectively. Via open-column chromatography, with $SiO_2$ as stationary

176 phase, fractionation of the extract was achieved by eluting the apolar fraction (HBIs) and the polar

177 fraction (sterols and GDGTs) with 5 ml n-hexane and 5 ml DCM/MeOH 1:1, respectively. The polar

178 fraction was subsequently split into two fractions (sterols and GDGTs) for further processing. The sterol

179 fraction was silylated with 300 µl bis-trimethylsilyl-trifluoroacetamide (BSTFA; 2h at 60 °C).

180 Compound analyses of HBIs and sterols were carried out on an Agilent Technologies 7890B gas

181 chromatograph (GC; fitted with a 30 m DB 1MS column; 0.25 mm diameter and 0.25 µm film thickness)

182 coupled to an Agilent Technologies 5977B mass selective detector (MSD; with 70 eV constant

hat formatiert: Englisch (Vereinigte Staaten)

hat formatiert: Englisch (Vereinigte Staaten)

183 ionization potential, ion source temperature of 230 °C). The GC oven was set to: 60 °C (3 min), 150 °C

184 (rate: 15 °C/min), 320 °C (rate: 10 °C/min), 320 °C (15 min isothermal) for the analysis of hydrocarbons

185 and to: 60 °C (2 min), 150 °C (rate: 15 °C/min), 320 °C (rate: 3 °C/min), 320 °C (20 min isothermal)

186 for the analysis of sterols. Helium was used as carrier gas. The ~~identification of~~ HBI and sterol

187 compounds ~~is based upon~~were identified by their GC retention times and mass spectra (Belt, 2018; Belt

188 et al., 2000; Boon et al., 1979). ~~Lipid quantification was obtained~~Lipids were quantified by setting the

189 individual, manually integrated, GC-MS peak area in relation to the peak area of the respective internal

190 standard and normalization to the amount of extracted sediment. ~~Quantification of~~IPSO$_{25}$ and HBI

191 trienes ~~was achieved using~~were quantified by relating their molecular ions (IPSO$_{25}$: m/z 348 and HBI

192 trienes: m/z 346) ~~in relation~~ to the fragment ion m/z 266 of the internal standard 7-HND (Belt, 2018).

193 ~~Quantification of sterols was achieved by comparison of~~Sterols were quantified by comparing the

194 molecular ion of the individual sterol with the molecular ion m/z 348 of the internal standard 5α-

195 androstan-3-ol. Instrumental response factors for the target lipids were considered as recommended by

196 Belt et al. (2014) and Fahl and Stein (2012). All biomarker concentrations were subsequently

197 normalized to the TOC content of each sample to account for different depositional settings within the

198 different study areas.

199 For calculating the phytoplankton-IPSO$_{25}$ (PIPSO$_{25}$) index, we used the equation introduced by Vorrath

200 et al. (2019);

201 PIPSO$_{25}$ = IPSO$_{25}$ / (IPSO$_{25}$ + (phytoplankton marker x c))                    (1)

202 where c (c = mean IPSO$_{25}$/mean phytoplankton marker) is applied as a concentration balance factor to

203 account for high concentration offsets between IPSO$_{25}$ and the phytoplankton biomarker (see Table S1

204 for c-factors of individual PIPSO$_{25}$ calculations).

205 Following the approach by Müller and Stein (2014) and Lamping et al. (2020), a PIPSO$_{25}$ value of 1

206 was assigned to samples with exceptionally low (at detection limit) concentrations of both biomarkers

207 ~~have been assigned a PIPSO$_{25}$ value of 1~~ (see chapter 4.1.2). This comprises the five Weddell ~~Seam~~Sea

208 samples PS111/13-2, /15-1, /16-3, /29-3 and /40-2 (marked as orange x in Fig. 1).

209 The GDGT fraction was dried under $N_2$, redissolved with 120 µl hexane:isopropanol (v/v 99:1) and

210 then filtered using a polytetrafluoroethylene (PTFE) filter with a 0.45 µm pore sized membrane. ~~GDGT~~

211 ~~measurements~~GDGTs were ~~carried out~~measured using high performance liquid chromatography

212 (HPLC; Agilent 1200 series HPLC system) coupled to an Agilent 6120 mass spectrometer (MS),

213 operating with atmospheric pressure chemical ionization (APCI). The injection volume was 20 µl. For

214 separating the GDGTs, a Prevail Cyano 3 µm column (Grace, 150 mm * 2.1 mm) was kept at 30 °C.

215 Each sample was eluted isocratically for 5 min with solvent A = hexane/2-propanol/chloroform; 98:1:1

216 at a flow rate of 0.2 ml/min, then the volume of solvent B = hexane/2-propanol/chloroform; 89:10:1

217 was increased linearly to 10 % within 20 min and then to 100 % within 10 min. The column was back-

218 flushed (5 min, flow 0.6 ml/min) after 7 min after each sample and re-equilibrated with solvent A (10

219 min, flow 0.2 ml/min). The APCI was set to the following: $N_2$ drying gas flow at 5 l/min and temperature

220 to 350 °C, nebulizer pressure to 50 psi, vaporizer gas temperature to 350 °C, capillary voltage to 4 kV

221 and corona current to +5 µA. Detection of GDGTs was achieved by means of selective ion monitoring

222 (SIM) of $[M+H]^+$ ions (dwell time 76 ms). ~~Determination and quantification of the molecular ions of~~

223 GDGT-0 (*m/z* 1302), GDGT-1 (*m/z* 1300), GDGT-2 (*m/z* 1298), GDGT-3 (*m/z* 1296) and crenarchaeol

224 (*m/z* 1292) as well as ~~of~~brGDGT-III (*m/z* 1050), brGDGT-II (*m/z* 1036) and brGDGT-I (*m/z* 1022) ~~was~~

225 ~~done in relation~~were quantified by relating their molecular ions to the molecular ion *m/z* 744 of the

226 internal standard $C_{46}$-GDGT. The late eluting hydroxylated GDGTs (OH-GDGT-0, OH-GDGT-1 and

227 OH-GDGT-2 with *m/z* 1318, 1316 and 1314, respectively) were quantified in the scans (*m/z* 1300, 1298,

228 1296) of their related GDGTs, as described by Fietz et al. (2013).

229 $TEX^L_{86}$ values and their conversion into SOTs were determined following Kim et al. (2012);

230 $$TEX^L_{86} = \cancel{LOG \frac{[GDGT-2]}{[GDGT-1]+[GDGT-2]+[GDGT-2]}} LOG \frac{[GDGT-2]}{[GDGT-1]+[GDGT-2]+[GDGT-3]} ,$$

231 $\hspace{6cm}$ (2)

232 $SOT^{TEX} [\,°C] = 50.8 \times TEX^L_{86} + 36.1.$ $\hspace{4cm}$ (3)

233 Temperature calculations based on OH-GDGTs were carried out according to Lü et al. (2015);

234 $$RI-OH' = \frac{[OH-GDGT-1]+2 \times [OH-GDGT-2]}{[OH-GDGT-0]+[OH-GDGT-1]+[OH-GDGT-2]} ,$$ $\hspace{2cm}$ (4)

235 $SST^{OH} [\,°C] = RI-OH' - 0.1/0.0382 .$ $\hspace{4cm}$ (5)

236 To determine the relative influence of terrestrial organic matter input, the Branched Isoprenoid

237 Tetraether (BIT)-index was calculated following Hopmans et al. (2004):

238 $$BIT = \frac{[brGDGT-I]+[brGDGT-II]+[brGDGT-III]}{[Chrenarchaeol]+[brGDGT-I]+[brGDGT-II]+[brGDGT-III]}. \tag{6}$$

239

240 ### 3.3 Numerical model

241 #### 3.3.1 Model description

242 AWI-ESM2 is a state-of-the-art coupled climate model developed by Sidorenko et al. (2019) which

243 comprises an atmospheric component ECHAM6 (Stevens et al., 2013) as well as an ocean-sea ice

244 component FESOM2 (Danilov et al., 2017). The atmospheric module ECHAM6 is the most recent

245 version of the ECHAM model developed at the Max Planck Institute for Meteorology (MPI) in

246 Hamburg. The model is branched from an early release of the European Center (EC) for Medium Range

247 Weather Forecasts (ECMWF) model (Roeckner et al., 1989). ECHAM6 dynamics is based on

248 hydrostatic primitive equations with traditional approximation. We used a T63 Gaussian grid which

249 haswith a spatial resolution of about 1.9 x 1.9 degree (1.9 ° or 210 km). There are 47 vertical layers in

250 the atmosphere.

251 Momentum transport arising from boundary effects is configured using the subgrid orography scheme

252 as described by Lott (1999). Radiative transfer in ECHAM6 is represented by the method described in

253 Iacono et al. (2008). ECHAM6 also contains a Land-Surface Model (JSBACH) which includes 12

254 functional plant types of dynamic vegetation and 2 bare-surface types (Loveland et al., 2000; Raddatz

255 et al., 2007). The ice-ocean module in AWI-ESM2 is based on the finite volume discretization

256 formulated on unstructured meshes. The multi-resolution for the ocean is up to 15 km over polar and

257 coastal regions, and 135 km for far-field oceans, with 46 uneven vertical depths. The impact of local

258 dynamics on the global ocean is related to a number of FESOM-based studies (Danilov et al., 2017).

259 The multi-resolution approach advocated by FESOM allows one to explore the impact of local

260 processes on the global ocean with moderate computational effort (Danilov et al., 2017). AWI-ESM2

261 employs the OASIS3-MCT coupler (Valcke, 2013) with an intermediate regular exchange grid.

262 Mapping between the intermediate grid and the atmospheric/oceanic grid is handled with bilinear

263 interpolation. The atmosphere component computes 12 air–sea fluxes based on four surface fields

264 provided by the ocean module FESOM2. AWI-ESM2 has been validated under modern climate

265 conditions (Sidorenko et al., 2019) and has been applied for marine radiocarbon concentrations

266 (Lohmann et al., 2020), the latest Holocene (Vorrath et al., 2020), and the Last Interglacial (Otto-

267 Bliesner et al., 2021).

268

269       3.3.2  Experimental design

270 One transient experiment was conducted using AWI-ESM2, which applied the boundary conditions,

271 including orbital parameters and greenhouse gases. Orbital parameters are calculated according to

272 Berger (1978), and the concentrations of greenhouse gases are taken from ice-core records as well as

273 from recentand measurements of recent firn air and atmospheric samples (Köhler et al., 2017). The

274 model was initialized from a 1,000-year spin-up run under mid-Holocene (6,000 before present, BP)

275 boundary conditions as described by Otto-Bliesner et al. (2017). In our modeling strategy, we follow

276 Lorenz and Lohmann (2004) and use the climate condition from the mid-Holocene spin-up run as the

277 initial state for the subsequent transient simulation covering the period from 6,000 BP to 2014 Common

278 Era (CE.). In the present study we derived seasonal SIC, SSTs and SOTs in the study areaareas from a

279 segment of the transient experiment (1950-2014 CE). Topography including prescribed ice sheet

280 configuration was kept constant in our transient simulation. All model data are provided in Table S2.

281

282       3.4.  Satellite SIC and SSTs

283 Satellite sea-ice data arewere derived from Nimbus-7 SMMR and DMSP SSM/I-SSMIS passive

284 microwave data and downloaded from the National Snow and Ice Data Center (NSIDC; Cavalieri et al.,

285 1996). The sea-ice data represent mean monthly SIC, which are expressed to range from 0 % to 100 %

286 and are averaged over a period of the beginning of satellite observations in 1978 CE to the individual

287 year of sample retrievalcollection. The monthly mean SIC were then split into different seasons: winter

288 (JJF), spring (SON) and summer (DJF) (Fig. 2a-c)), and thethese data are considered to represent the

289 recent mean state of sea-ice coverage. All satellite data are provided in Table S3.

290 Modern annual mean SSTs and SOTs ~~are~~were derived from the World Ocean Atlas ~~13 representing~~2013

291 and represent averaged values for the years 1955-2012 CE (WOA13; Locarnini et al., 2013).

292

## 4. Results and discussion

294 In the following, we first present and discuss the biomarker data ~~assembled during~~generated for this

295 study from North (Antarctic Peninsula) to South (Amundsen and Weddell ~~Seas~~seas) and draw

296 conclusions about the environmental settings deduced from the data set. ~~As~~ In regard to the

297 phytoplankton-derived biomarkers, we ~~here~~ focus on the significance of HBI Z-triene and

298 brassicasterol, ~~while~~because the HBI E-triene and dinosterol ~~showing~~data, which are presented in the

299 supplementary material (Fig. S1), show very similar patterns ~~are moved to the supplement (Fig. S1)~~

300 ~~to avoid repetition.~~. All biomarker data ~~collected during this study~~ are provided in Table S1 and are

301 available ~~via~~from the PANGAEA data repository (DOI in prep.). For the discussion of the target

302 environmental variables, *i.e.* PIPSO$_{25}$-based sea-ice and GDGT-derived ocean temperature estimates,

303 satellite ~~and,~~ instrumental ~~as well as modelled~~and model data are considered. In ~~Sect.~~section 5, we

304 further address potential caveats in biomarker-based environmental reconstructions that need to be

305 ~~considered~~taken into account when applying these proxies.

306

### 4.1 TOC content, HBIs and sterols in Antarctic surface sediments

308 TOC contents in marine sediments ~~in a first approximation~~ are often viewed as an indicator for primary

309 productivity in surface waters (Meyers, 1997). However, we are aware that additional factors, such as

310 different water depths ~~or~~and depositional regimes, may exert control on sedimentary TOC as well. The

311 TOC contents of the ~~herein~~ investigated surface samples are lowest in Drake Passage with values around

312 0.12-0.54 ~~%, increasing in a~~% and increase from northwest to southeast ~~gradient~~ into Bransfield Strait,

313 ~~ranging between~~where they range from 0.59 ~~and~~to 1.06 % (Fig. 3a; WAP). ~~At~~Along the EAP, higher

314 TOC contents (0.57-0.86 %) prevail around the former Larsen A Ice Shelf ~~with a decreasing trend~~and

315 north of James Ross Island but they decrease towards ~~the~~ Powell Basin (0.22-0.37 %) and ~~an~~then

316 increase to 0.50 % around ~~the area of~~ the South Orkney Islands, which may point to elevated

13

317 productivity or enhanced supply of reworked terrigenous organic matter in ~~these areas~~this area (Fig. 3a;
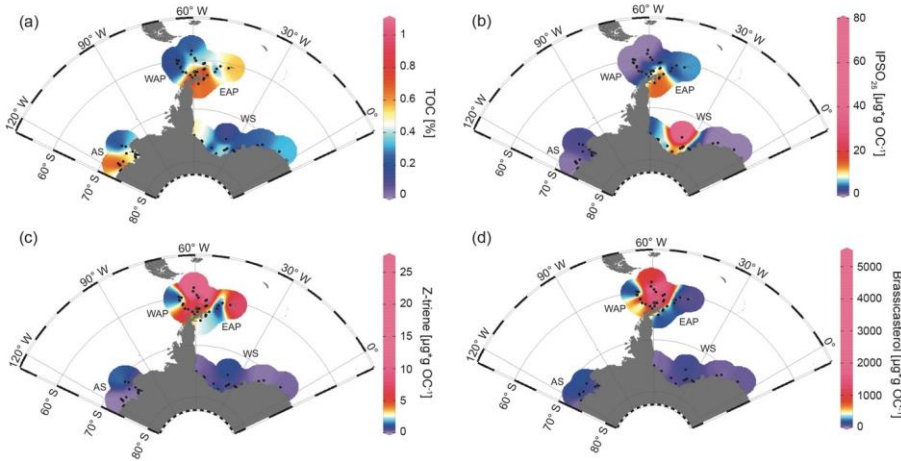
318 EAP).

**Fig. 3:** Distribution of (a) TOC [%], (b) IPSO$_{25}$, (c) Z-triene and (d) brassicasterol in surface sediment samples. Sample locations are marked as black dots. Concentrations of biomarkers [µg*g OC$^{-1}$] were normalized to the TOC content of each sample. AS: Amundsen Sea, WAP: West Antarctic Peninsula, EAP: East Antarctic Peninsula, WS: Weddell Sea.

319 At the WAP, concentrations of the sea-ice biomarker IPSO$_{25}$ ~~show a~~increase from northwest~~-~~ to

320 southeast ~~gradient with~~. IPSO$_{25}$ ~~being~~is absent in samples from the permanently ice-free Drake Passage

321 and ~~increasing concentrations~~increases towards the continental slope and the seasonally ice-covered

322 ~~continental~~ shelf (0.37-17.81 µg*g OC$^{-1}$; Fig. 3b; Vorrath et al., 2019). Highest IPSO$_{25}$ concentrations

323 are observed in samples of the northern Bransfield Strait~~, which is affected by~~. Here, the inflow of

324 ~~water masses~~waters from the Weddell Sea ~~through the Antarctic Sound and along the Antarctic~~

325 ~~Peninsula and frequent transport of~~transports sea ice into ~~the~~ Bransfield Strait (Vorrath et al., 2019).

326 Elevated IPSO$_{25}$ concentrations are also observed at the ~~EAP, influenced by a seasonal~~seasonally sea-

327 ice ~~cover~~covered EAP, where relatively ~~higher~~high concentrations of the sea-ice biomarker prevail in

328 ~~those~~ samples located in ~~front~~the area of the former Larsen A Ice Shelf and north of James Ross Island

329 (12.59-17.74 µg*g OC$^{-1}$; Fig. 3b). ~~As~~Because these locations are ~~also~~ influenced by the northward drift

330 of sea ice within the Weddell Gyre (Fig. 1), the elevated IPSO$_{25}$ concentrations could also result from

331 sea ice advected from the southern Weddell Sea. We suggest that the ~~decreasing~~decrease of IPSO$_{25}$

332  concentrations towards the Powell Basin and the South Orkney Islands (0.59-5.36 µg*g OC$^{-1}$; Fig. 3b)

333  ~~can be~~is connected to warmer ocean temperatures ~~towards~~in the North and ~~less~~reduced sea-ice

334  ~~coverage~~cover during spring.

335  Concentrations of the phytoplankton biomarker HBI Z-triene around the Antarctic Peninsula are highest

336  in ~~the~~ eastern Drake Passage and along the WAP continental slope (where IPSO$_{25}$ is absent) and

337  decrease in ~~the~~ Bransfield Strait (0.33-26.86 µg*g OC$^{-1}$; Fig. 3c; Vorrath et al., 2019). Elevated HBI Z-

338  triene concentrations have ~~thus~~, so far, been detected in surface waters along ~~an~~the sea-ice edge (Smik

339  et al., 2016) and hence were suggested to be a proxy for marginal ice zone conditions (Belt et al., 2015;

340  Collins et al., 2013; Schmidt et al., 2018),. Vorrath et al. (2019), however, relate the high concentrations

341  of HBI Z-triene at the northernmost stations in the permanently ice-free eastern Drake Passage to their

342  proximity to the Antarctic Polar Front. Here, productivity of the source diatoms of HBI-trienes (*e.g.*,

343  *Rhizosolenia* spp.; Belt et al., 2017) may be enhanced by meander-induced upwelling leading to

344  increased nutrient flux to surface waters (Moore and Abbott, 2002). Since Cardenas et al. (2019)

345  document only minor abundances of *Rhizosolenia* spp. in seafloor surface sediments from this area, we

346  assume that HBI-trienes might also be biosynthesized by other ~~diatoms~~diatom taxa. Moderate

347  concentrations along the continental slope of the WAP and in ~~the~~ Bransfield Strait ~~have been~~were

348  associated with elevated inflow of warm BSW which leads to a retreating sea-ice margin during spring

349  and summer (for more details, see Vorrath et al., 2019; 2020). Samples from the EAP ~~continental~~ shelf

350  and ~~the~~ Powell Basin are characterised by relatively low HBI Z-triene concentrations ~~of HBI Z-triene~~

351  (Fig. 3c; 0.1-2.37 µg*g OC$^{-1}$~~), showing a~~) that decrease from southwest- to northeast ~~gradient, while~~,

352  whereas the northernmost sample closest to the South Orkney Islands is characterized by an elevated

353  HBI Z-triene concentration of ~8.49 µg*g OC$^{-1}$ (Fig. 3c; EAP). This relatively high concentration may

354  be related to an "Island Mass Effect", coined by Doty and Oguri (1956), which refers to ~~an~~ increased

355  primary production around oceanic islands in comparison to surrounding waters. Nolting et al. (1991)

356  found extraordinarily high dissolved iron levels (as high as 50-60 nM) on the ~~shelf of the~~ South Orkney

357  ~~Islands, and~~shelf, while Nielsdóttir et al. (2012) observed enhanced iron and Chl *a* concentrations in the

358  vicinity of the South Orkney Islands. These authors explain the increased dissolved iron levels with

359  input from seasonally retreating sea ice, which is recorded by satellites (Fig. 2a-c) and probably leads

hat formatiert: Schriftart: 11 Pt., Englisch (Vereinigtes Königreich)

hat formatiert: Schriftart: 11 Pt., Englisch (Vereinigte Staaten)

to substantial annual phytoplankton blooms, which may also cause the elevated TOC content in the corresponding seafloor sediment sample (Fig. 3a). Alternatively, remobilization of shelf sediments or vertical mixing of iron-rich deep waters, leading to high iron contents in surface waters, may stimulate primary productivity (Blain et al., 2007; de Jong et al., 2012). However, it remains unclear why the brassicasterol concentration is distinctly low in this sample, and we assume that different environmental preferences of the source organisms may account for this. In Drake Passage and along the EAP, brassicasterol displays a similar pattern as ~~the~~ HBI Z-triene, with relatively high concentrations (more than 2 orders of magnitudes~~),~~) ranging ~~between~~from 1.86 ~~and~~to 5017.44 µg*g OC$^{-1}$ (Fig. 3d).

In the Weddell Sea, TOC contents are generally ~~lower~~low (< 0.4 %), with slightly elevated values in the West (up to 0.50 %) and right in front of the Filchner Ice Shelf (up to 0.52 %; Fig. 3a). The Amundsen Sea is characterized by slightly higher TOC contents, with concentrations of up to 0.91 % in the West and lower values in the East (0.33 %; Fig. 3a; AS).

In the samples from the Amundsen and Weddell ~~Seas,~~seas, that both are dominated by ~~a~~ strong winter sea-ice cover lasting until spring (Fig. 2a-c), all three biomarkers are present in low concentrations only. An exception are the samples located in front of the Filchner Ice Shelf with significantly higher concentrations of IPSO$_{25}$ (7.09-73.87 µg*g OC$^{-1}$; Fig. 3b; WS). Concentrations of IPSO$_{25}$ on the Amundsen Sea shelf are relatively low (0.04-3.3 µg*g OC$^{-1}$), with slightly higher values observed ~~towards~~in the north-east (Fig. 3b; AS). HBI Z-triene ~~is~~concentrations are also very low ~~concentrated, showing,~~ but slightly higher ~~concentrations~~ in Filchner Trough (0.04-1 µg*g OC$^{-1}$) and ~~towards the~~at more distal locations ~~in~~on the northeastern Amundsen Sea shelf (0.01-1.88 µg*g OC$^{-1}$; Fig. 3c). Brassicasterol generally shows a similar ~~patterns~~pattern as ~~the~~ HBI Z-triene, with concentrations ~~ranging~~varying between 1.86 and 220.54 µg*g OC$^{-1}$ (Fig. 3d; for HBI E-triene and dinosterol distribution, see Fig. S1).

### 4.2 Combining individual biomarker records: the PIPSO$_{25}$ index

The PIPSO$_{25}$ index combines the relative concentrations of IPSO$_{25}$ and a selected phytoplankton biomarker, such as HBI-trienes and sterols, as indicator for an open-ocean environment (Vorrath et al., 2019). The combination of both end members (sea ice vs. open-ocean) prevents misleading

388 interpretations regarding the absence of IPSO$_{25}$ in the sediments, which can be the result of two entirely

389 different scenarios. ~~At~~Under heavy/perennial sea-ice ~~conditions~~coverage, the thickness of sea ice

390 hinders light penetration, thereby limiting the productivity of algae living in basal sea ice (Hancke et

391 al., 2018). This scenario ~~may~~can cause the absence of both phytoplankton and sea-ice biomarkers in the

392 sediment. The other scenario depicts a permanently open ocean, where the sea-ice biomarker is absent

393 as well, but here~~,~~ the phytoplankton biomarkers are present in variable concentrations (Müller et al.,

394 2011). The presence of both biomarkers in the sediment is indicative of seasonal sea-ice coverage and/or

395 the occurrence of stable sea-ice margin conditions, promoting biosynthesis of both biomarkers (Müller

396 et al., 2011). We here distinguish between P$_Z$IPSO$_{25}$ and P$_B$IPSO$_{25}$ using HBI Z-triene and brassicasterol

397 as phytoplankton biomarker, respectively (Fig. 4a+b; for PIPSO$_{25}$ values based on HBI E-triene and

398 dinosterol see Table S1 and Fig. S2).
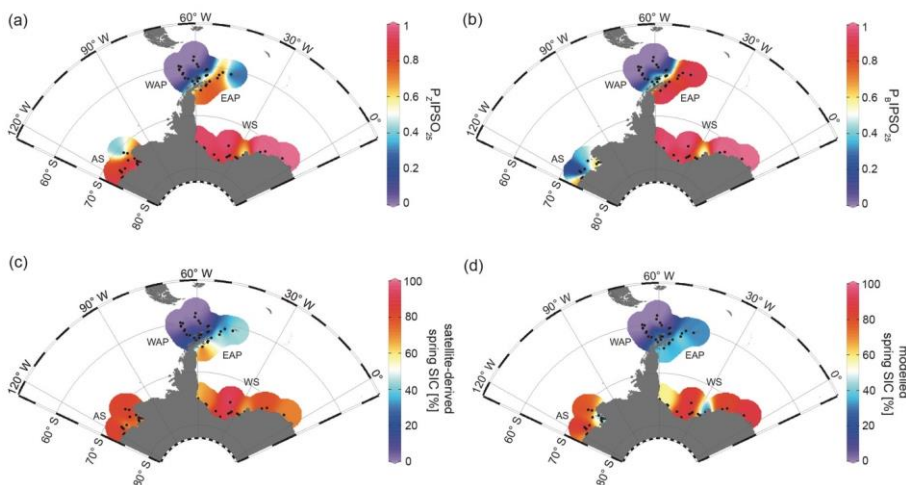


**Fig. 4:** Distribution of the sea-ice index PIPSO$_{25}$ in surface sediment samples, with (a) P$_Z$IPSO$_{25}$ based on Z-triene and (b) P$_B$IPSO$_{25}$ based on brassicasterol, (c) satellite-derived spring SIC [%] and (d) modelled spring SIC [%]. AS: Amundsen Sea, WAP: West Antarctic Peninsula, EAP: East Antarctic Peninsula, WS: Weddell Sea.

399 Both PIPSO$_{25}$ indices are 0 in the predominantly ice-free Drake Passage and ~~display a northwest~~

400 increase towards southeast ~~gradient~~to intermediate values ~~towards~~on the ~~continental~~WAP slope and

401 around the South Shetland Islands, reflecting increased influence of marginal sea-ice cover towards the

402 coast (0.02-0.70; Vorrath et al., 2019). At the seasonally sea-ice covered EAP, P$_Z$IPSO$_{25}$ values reach

403 0.84, while lower values of around 0.25 are observed close to the South Orkney Islands, which ~~relates to~~is caused by the elevated HBI Z-triene concentrations at the stations there (Fig. 3c; EAP). The

405 $P_BIPSO_{25}$ index exhibits even higher values of up to 0.98 at the EAP/northwestern Weddell Sea. These

406 elevated $PIPSO_{25}$ indices align well with the significant northward sea-ice- drift within the Weddell

407 Gyre ~~in that region~~, which leads to prolonged sea-ice cover along the EAP.

408 In samples from the southern Weddell Sea, both $PIPSO_{25}$ indices show a similar pattern with high values

409 up to 0.9, and slightly lower values in front of the Brunt Ice Shelf (0.6; Fig. 4a+b). Very low

410 concentrations (close to detection limit) of both biomarkers in samples ~~located on~~from the continental

411 shelf off Dronning Maud Land (Fig. 1) result in low $PIPSO_{25}$ values, strongly underestimating the sea-

412 ice cover in ~~that~~this area. ~~Regarding the~~, where satellite-derived sea-ice data~~, this area of the continental~~

413 ~~shelf is influenced by a~~ document severe seasonal sea-ice cover (Fig. 2). As previously mentioned, we

414 followed the approach by Müller and Stein (2014) and Lamping et al. (2020) ~~and assigned~~by assigning

415 a maximum $PIPSO_{25}$ value of 1 to these samples to circumvent misleading interpretations and aid

416 visualisation.

417 The intermediate $PIPSO_{25}$ value (~0.51) derived for one sample collected in front of the Brunt Ice Shelf

418 points to a less severe sea-ice cover in that area. A possible explanation for the relatively ~~lower~~low

419 $PIPSO_{25}$ value ~~may be~~is the presence of a coastal polynya that has been reported by Anderson (1993)

420 and which is further supported by Paul et al. (2015~~), who~~). These authors note that the sea-ice area

421 around the Brunt Ice Shelf is the most active in the southern Weddell Sea, with an annual average

422 polynya area of 3516 ± 1420 km². Interestingly, the reduced SIC here is also captured by our model

423 (see ~~Sect.~~section 4.3).

424 $PIPSO_{25}$ values in the Amundsen Sea point to different scenarios. The $P_ZIPSO_{25}$ index ~~ranges~~varies

425 around 0.9, with only the easterly, more distal ~~locations showing~~samples having lower values between

426 0.3 and 0.6 (Fig. 4a). The $P_BIPSO_{25}$ index generally ~~presents~~has lower values, ranging from 0.6 in the

427 coastal area to 0.2 in the more distal samples (Fig. 4b). This difference between $P_ZIPSO_{25}$ and $P_BIPSO_{25}$

428 may be explained by the different source organisms biosynthesizing the individual phytoplankton

429 biomarkers. While the main origin of HBI-trienes seems to be restricted to diatoms (Belt et al.,

18

430  2017), brassicasterol is known to be produced by several algal groups that are adapted to a wider range

431  of sea surface conditions (Volkman, 2006; see ~~Sect.~~section 5.2).

432

### 4.3  Biomarker-based sea ice estimates vs. satellite and model data

434  The main ice algae bloom in the Southern Ocean occurs during spring, when solar insolation and air

435  temperatures/SSTs increase and sea ice starts ~~melting~~to melt, which results in the release of nutrients

436  and stratification of the water column stimulating the productivity of photosynthesizing organisms

437  (Arrigo, 2017; Belt, 2018). The sea-ice biomarker $IPSO_{25}$ is hence commonly interpreted as a spring

438  sea-ice indicator, which is why, in the following, we compare the biomarker-based sea-ice

439  reconstructions to satellite-derived and modelled spring SIC. $IPSO_{25}$ concentrations in the surface

440  sediments around the Antarctic Peninsula exhibit similar trends as the satellite-derived and modelled

441  SIC (Figs. 3+4), while they differ significantly in the Amundsen and Weddell ~~Seas~~seas, where high SIC

442  are ~~depicted~~recorded by satellites and the model but $IPSO_{25}$ is ~~very~~present in low

443  ~~concentrated.~~concentrations. The low $IPSO_{25}$ concentrations in these areas highlight the uncertainty,

444  when considering $IPSO_{25}$ as a sea-ice proxy alone, since such low concentrations are not only observed

445  under open water conditions, but also under ~~a~~ severe sea-ice cover. In ~~this case~~the Amundsen and

446  Weddell seas, the low $IPSO_{25}$ concentrations ~~of IPSO₂₅~~ are the result of the latter, where limited light

447  availability hinders ice algae growth, leading to an underestimation of sea-ice cover. Accordingly, we

448  note a weak correlation between $IPSO_{25}$ data and satellite SIC ($R^2 = 0.19$; Fig. 5a). As stated above, the

449  combination of $IPSO_{25}$ and a phytoplankton marker may prevent this ambiguity. The higher sea-ice

450  concentrations in the Amundsen and Weddell ~~Seas~~seas are better reflected by maximum $P_ZIPSO_{25}$

451  values than by $IPSO_{25}$ alone. However, we note that the $P_ZIPSO_{25}$ index ~~seems to~~apparently does not

452  ~~further~~ resolve SICs higher than 50 % (see Fig. S3), which may indicate a threshold (here ~50 % SIC)

453  where the growth of the HBI- triene and $IPSO_{25}$ producing algae is limited.
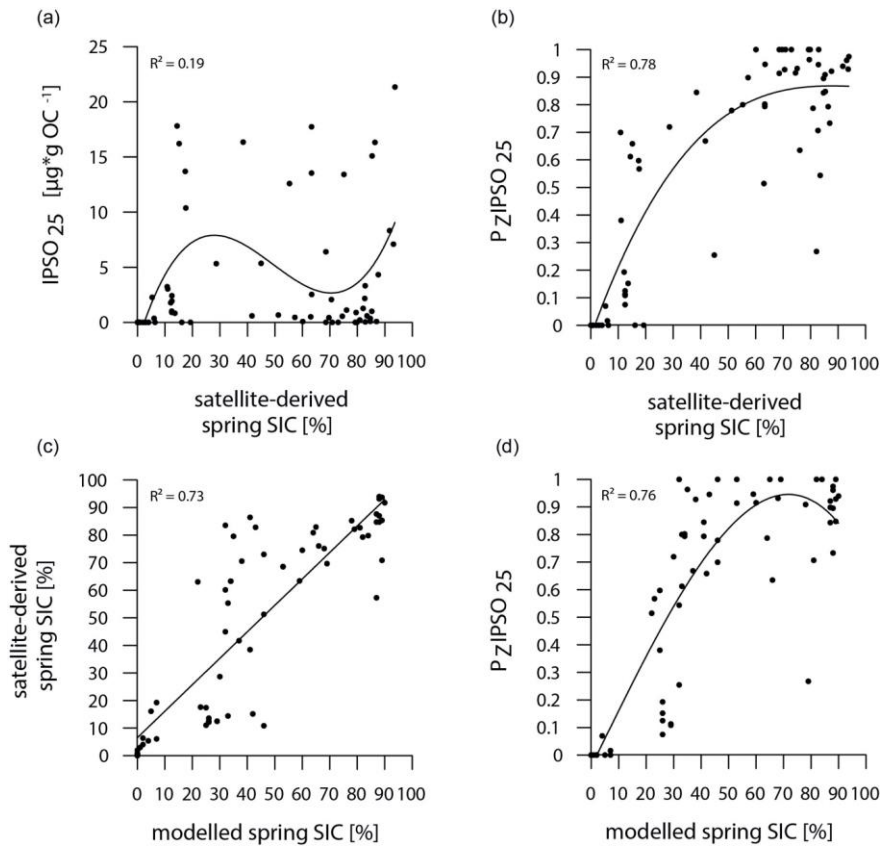
**Fig. 5:** Correlations of (a) IPSO$_{25}$ concentrations vs. satellite-derived spring SIC, (b) P$_Z$IPSO$_{25}$ values vs. satellite-derived spring SIC, (c) satellite-derived spring SIC vs. modelled spring SIC and (d) P$_Z$IPSO$_{25}$ values vs. modelled spring SIC. Coefficients of determination (R$^2$) are given for the respective regression lines.

454     In general, however, the P$_Z$IPSO$_{25}$ values correlate much better with satellite and modelled SIC (R² =

455     0.78 and R$^2$ = 0.76, respectively; Fig. 5b+d) than IPSO$_{25}$ concentrations. Correlations of satellite and

456     model data with PIPSO$_{25}$ calculated using the HBI E-triene, brassicasterol and dinosterol, respectively,

457     are also positive but less significant (Fig. S4~~)~~)), and we hence focus the discussion on P$_Z$IPSO$_{25}$.The

458     AWI-ESM2-derived spring SICs correctly display the permanently ice-free Drake Passage and the

459     northwest-southeast ~~gradient~~increase in sea-ice cover from the WAP continental slope towards ~~the~~

460     Bransfield Strait (Fig. 4d). The model, however, significantly underestimates the elevated sea-ice

461     concentrations (up to 70 %) in front of the former Larsen Ice Shelf A and east of James Ross Island at

20

462 the EAP ~~depicted by~~_observed in_ satellite data. In the Amundsen and Weddell ~~Seas~~_seas_, the model ~~shows~~

463 ~~a~~_predicts_ heavy sea-ice cover (~90 %), only slightly underestimating the sea-ice cover at the near-

464 coastal sites in front of Pine Island Glacier and ~~the~~ Ronne Ice Shelf. Interestingly, modelled SIC in ~~the~~

465 ~~area in~~ front of ~~the~~ Brunt Ice Shelf is as low as ~45 % (Fig. 4d+e), corresponding well with the reduced

466 $P_ZIPSO_{25}$ value of ~0.51~~, and~~_. This_ may reflect the polynya conditions in that region documented by

467 Anderson (1993) and Paul et al. (2015). Overall, we note that modelled modern SICs correlate well with

468 satellite data ($R^2 = 0.73$; Fig. 5c) and $P_ZIPSO_{25}$ values ($R^2 = 0.76$; Fig. 5d), while we observe weaker

469 correlations between modelled paleo-SICs and $P_ZIPSO_{25}$ values (Fig. S5; see ~~Sect.~~_section_ 5.1).

470

471      4.4   $TEX^L_{86}$ and RI-OH'-_-_derived ocean temperatures

472 For a critical appraisal of the applicability and reliability of GDGT indices as temperature proxies in

473 polar latitudes, we here focus on the $TEX^L_{86}$ proxy by Kim et al. (2012), _which_ potentially

474 ~~reflecting~~_reflects_ SOTs, and the RI-OH' proxy~~,~~ _by Lü et al. (2015), which is_ assumed to reflect SSTs~~,~~

475 ~~by Lü et al. (2015).~~ _._ The reconstructions are ~~considered~~_believed_ to represent annual mean ocean

476 temperatures (for correlations of $TEX^L_{86}$-derived SOTs with WOA spring and winter SOTs, see Fig.

477 S6). In all samples, the BIT-index (Eq. 6) is <0.3, indicating no significant ~~contribution~~_impact_ of

478 terrestrial input ~~influencing~~_of organic material on_ the distribution _of GDGTs_ and hence ~~applicability of~~

479 ~~GDGTs to estimate ocean temperatures~~_their reliability as temperature proxy_. RI-OH'-derived

480 temperatures and $TEX^L_{86}$-derived SOTs both show a similar pattern, but different temperatures

481 ~~ranging~~_ranges_ between -2.62 to +4.67 °C and -2.38 to +8.75 °C, respectively (Fig. 6a+b). At the WAP,

482 RI-OH'- as well as $TEX^L_{86}$-derived temperatures ~~follow a northwest-southeast gradient with higher~~

483 ~~temperatures in~~_increase northwestwards across the Antarctic continental slope and into_ the permanently

484 ice-free Drake Passage ~~and on the Antarctic continental slope~~_, which are_ influenced by the ACC and

485 relatively warm CDW (Orsi et al., 1995; Rintoul et al., 2001). Temperatures decrease towards ~~the~~

486 Bransfield Strait and the EAP, which are influenced by ~~a~~ seasonal sea-ice cover and relatively ~~colder~~

487 ~~and highly saline~~_cold_ water from the Weddell Sea~~, branching~~ _that branches_ off the Weddell Gyre

488 (Collares et al., 2018; Thompson et al., 2009). At the EAP, a ~~southwest-northeast gradient can~~

489 ~~be~~southwestward decrease is observed, with relatively ~~lower~~low temperatures ~~along~~at the former

490 Larsen A Ice Shelf and higher temperatures ~~towards the~~recorded in Powell Basin and around the South
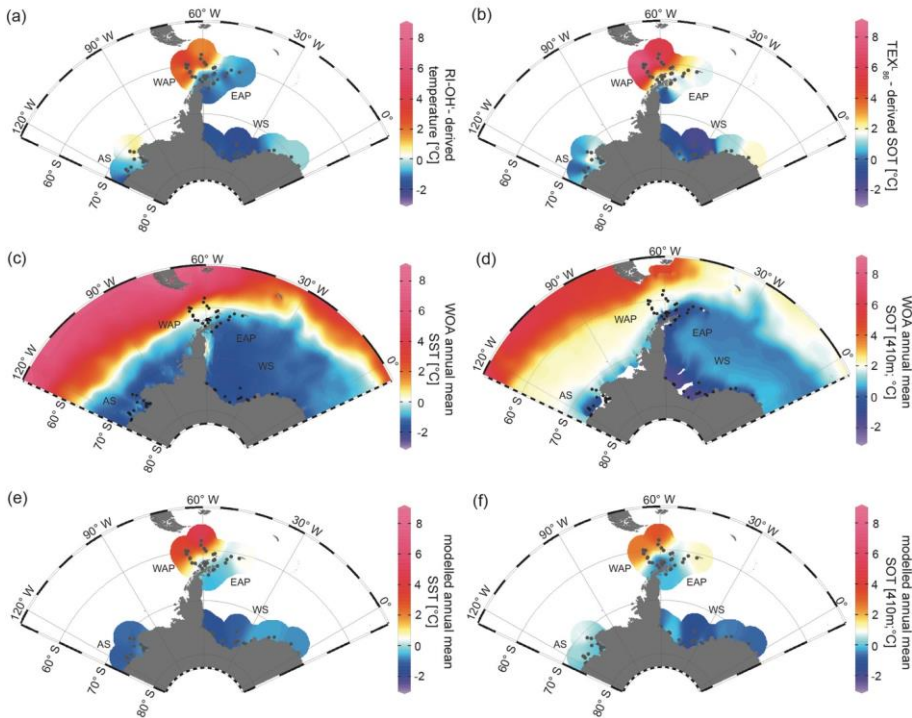
491 Orkney Islands (Fig. 6a+b).



**Fig. 6:** Annual mean temperature distributions with (a) RI-OH´-derived temperature, (b) TEX$^L_{86}$-derived SOT, (c) WOA13 SST (Locarnini et al., 2013), (d) WOA13 SOT (410 m; Locarnini et al., 2013), (e) modelled SST and (f) modelled SOT (410 m) in °C. AS: Amundsen Sea, WAP: West Antarctic Peninsula, EAP: East Antarctic Peninsula, WS: Weddell Sea.

492 ~~Further to the South, in~~In the Amundsen and Weddell ~~Seas,~~seas further south, reconstructed

493 temperatures are generally lower than ~~at~~around the Antarctic Peninsula. Samples from the Weddell Sea

494 display a temperature decrease from east to west, which may reflect the ~~eddy-driven~~ route of eddies

495 in the ~~north-eastern corner of the~~northeastern Weddell Gyre ~~carrying~~. These eddies carry relatively

496 warm, salty CDW~~, which then advects~~ westward along the southern ~~edge~~limb of the Weddell Gyre~~as,~~

497 where it becomes WDW (Vernet et al., 2019). Coldest TEX$^L_{86}$ ~~as well as~~and RI-OH' temperatures

hat formatiert: Englisch (Vereinigte Staaten)

498  (<0 °C) at sites along the Filchner-Ronne Ice Shelf front may be further linked to the presence of cold

499  precursor water masses for WSBW.

500  With regard to ongoing discussions, whether GDGT-based temperature reconstructions represent SSTs

501  or SOTs (Kalanetra et al., 2009; Kim et al., 2012; Park et al., 2019), we here compare our RI-OH' and

502  TEX$^L_{86}$-derived temperatures with ~~instrumental and modelled~~ surface ~~as well as~~and subsurface

503  temperature data obtained by in-situ measurements and modelling (Fig. 6c-f). ~~Based on~~

504  ~~correlations~~Comparison of GDGT-derived temperatures with WOA13 temperatures ~~reflecting~~from

505  different water depths~~, we observe~~ reveals the ~~highest significance at~~most significant correlation for a

506  water depth of 410 m (for respective correlations, see Fig. S7). When discussing instrumental and

507  modelled SOTs, we hence refer to 410 m water depth.
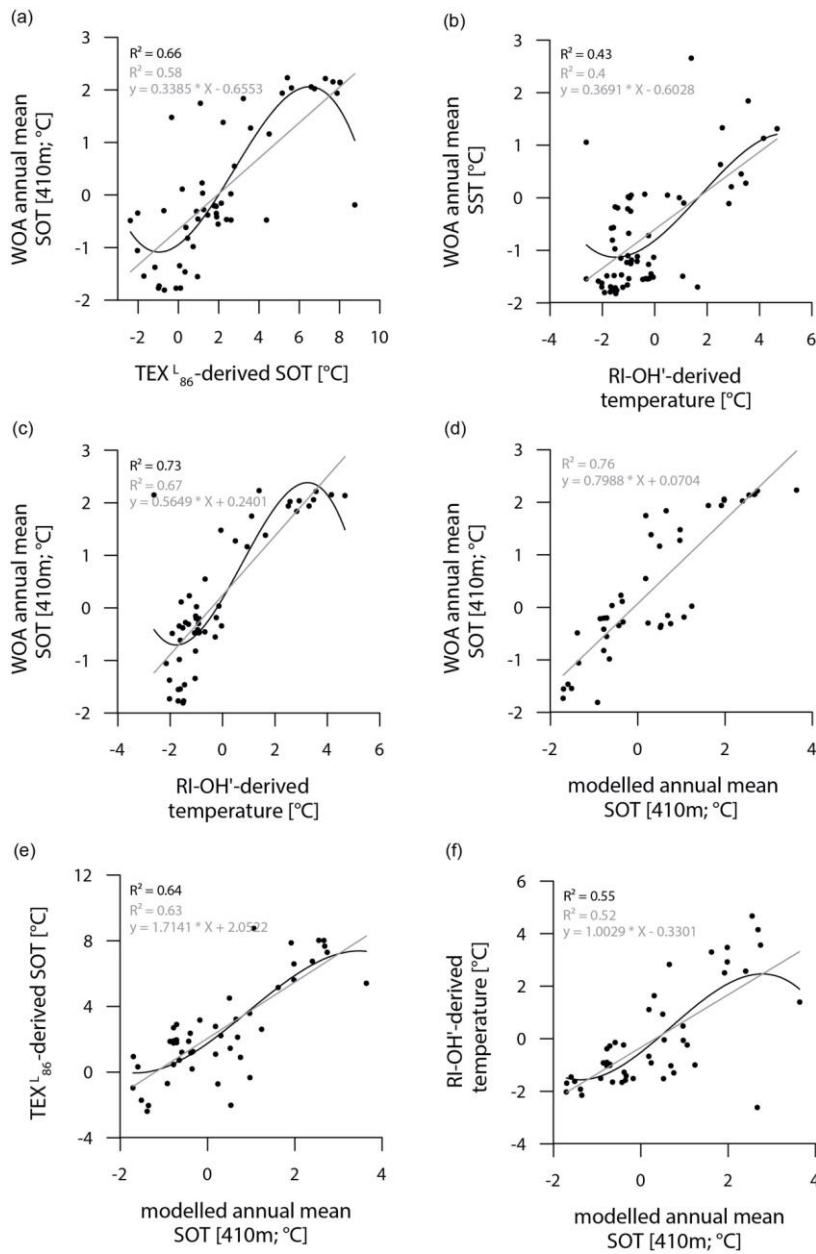
**Fig. 7:** Correlations of (a) WOA annual mean SOT (410 m) vs. TEX$^L_{86}$-derived SOT, (b) WOA annual mean SST vs. RI-OH'-derived temperature, (c) WOA annual mean SOT (410 m) vs. RI-OH'-derived temperature, (d) WOA annual mean SOT (410 m) vs. modelled annual mean SOT (410 m), (e) TEX$^L_{86}$-derived SOT vs. modelled annual mean SOT (410 m), (f) RI-OH'-derived temperature vs. modelled annual mean SOT (410 m) in °C. Coefficients of determination (R$^2$) are given for the respective regression lines.

508  While the correlation between $TEX^L_{86}$-derived SOTs and instrumental SOTs is reasonably ~~well~~good

509  (Fig. 7a; $R^2 = 0.66$), also supporting ~~the assumption of~~ a subsurface origin for the $TEX^L_{86}$ proxy, we

510  note a significant overestimation of SOTs by up to 6 °C in ~~the~~ Drake Passage (Fig. S8). This warm-

511  biased $TEX^L_{86}$ signal is a known caveat and is, among others, assumed to be connected to GDGTs

512  produced by deep-dwelling Euryarchaeota (Park et al., 2019), which have been reported in CDW

513  (Alonso-Sáez et al., 2011) and in deep waters at the Antarctic Polar Front (López-García et al., 2001).

514  Maximum $TEX^L_{86}$-based SOTs of 5 °C - 8 °C in ~~the~~ central Drake Passage (Fig. 6b), however, distinctly

515  exceed the common temperature range of CDW (0-2 °C). Interestingly, $TEX^L_{86}$-derived SOTs in the

516  colder regions of the Amundsen and Weddell ~~Seas~~seas relate reasonably well to instrumental

517  temperatures and are only slightly warm-biased (Fig. S8). Correlations between RI-OH'-derived

518  temperatures ~~with~~and instrumental SSTs are ~~comparatively~~ weak ($R^2 = 0.43$; Fig. 7b). Recently, Liu et

519  al. (2020) concluded in their study on surface sediments from Prydz Bay (East Antarctica), that also the

520  RI-OH' index holds promise as a tool to reconstruct SOTs rather than SSTs. When correlating our RI-

521  OH'-derived temperatures with instrumental SOTs, we similarly find a high correlation ($R^2 = 0.73$; Fig.

522  7c), ~~too,~~hence supporting this hypothesis. We further note that the RI-OH' temperature range ~~of RI-~~

523  ~~OH'~~ is much more realistic than the $TEX^L_{86}$~~, supporting the study by Park et al. (2019) and~~

524  ~~demonstrating~~ range. This suggests that the addition of OH-isoGDGTs in the temperature index is a

525  promising step towards reliable high latitude temperature reconstructions and may improve our

526  understanding of the temperature responses of archaeal membranes in Southern Ocean waters (Fietz et

527  al., 2020; Park et al., 2019). Clearly, more data – ideally obtained from sediment traps, seafloor surface

528  sediment samples ~~as well as~~and longer sediment cores – and calibration studies will help to further

529  elucidate the applicability of ~~this approach~~the RI-OH' and $TEX^L_{86}$ temperature reconstructions.

530  Similar to the model-derived sea-ice data, we ~~here~~ also evaluate the model's performance in depicting

531  ocean temperatures (Fig. 6e+f). Modelled annual mean SSTs and SOTs are highest (with up to 5 °C and

532  3 °C, respectively~~.~~) in the permanently ice-free Drake Passage, which is influenced by the relatively

533  warm ACC. ~~Decreasing~~Lower SSTs are ~~simulated towards~~predicted for the Antarctic Peninsula

534  continental slope and ~~the~~ Bransfield Strait (~0.5 to 1 °C), coinciding with the increase in the duration

25

535 of seasonal sea-ice cover in that area. At the EAP/northwestern Weddell Sea, modelled SSTs as well as

536 SOTs ~~show a~~increase from southwest~~-~~ to northeast ~~directed increase~~ towards Powell Basin. In the

537 Amundsen and Weddell ~~Seas~~seas, annual mean SSTs are negative, with temperatures ranging from -1

538 to -0.5 °C, while SOTs are positive in the Amundsen Sea and negative in the Weddell Sea. Overall, we

539 note that modelled SOTs reflect instrumental SOTs reasonably well ($R^2 = 0.76$; Fig. 7d). Interestingly,

540 while RI-OH'-derived SOTs relate better to instrumental SOTs (than $TEX^L_{86}$-based SOTs), ~~we note~~ a

541 better correlation between $TEX^L_{86}$-derived SOTs and modelled SOTs ($R^2 = 0.64$; Fig. 7e) and a weaker

542 correlation with Ri-OH'-derived temperatures ($R^2 = 0.55$; Fig. 7f~~.~~) is found.

543

544 **5. Caveats and recommendations for future research**

545 Marine core top studies ~~to elucidate~~evaluating the applicability and reliability of climate proxies are

546 often ~~concerned with~~affected by limitations and uncertainties regarding the age control of the

547 investigated seafloor surface sediments as well as the production, preservation and degradation of target

548 compounds. In the following, we shortly address some of these factors and provide brief

549 recommendations for future investigations.

550

551 5.1 Age control

552 Information on the actual age of the surface ~~sediments are~~sediment samples is a major requirement

553 determining their suitability to reflect modern sea surface conditions. When comparing sea-ice

554 conditions or ocean temperatures estimated from ~~sedimentary~~ biomarker data obtained from 0.5-1 cm

555 thick surface sediment samples (easily spanning decades to millennia, depending on sedimentation

556 rates) with satellite-derived sea-ice data or instrumental records (covering only the past ~40 and 65

557 years, respectively), the different time periods reflected in the data sets need to be considered when

558 interpreting the results. To address the issue of lacking age constraints for most of the ~~herein studied~~

559 surface sediments investigated here, we also performed paleoclimate simulations providing sea-ice

560 concentration data for three time slices (2 ka, 4 ka and 6 ka BP; see Fig. S5) to evaluate~~,~~ if the surface

561 sediments may have recorded significantly older environmental conditions. Correlations of $PIPSO_{25}$

values ~~against~~with these paleo ~~time slice~~ sea-ice concentrations ~~depicted~~are notably weaker ~~relations~~ (Fig. S5) ~~compared to~~than the correlations with recent (1951-2014 CE) SIC model output, which points to a ~~relatively~~ young to modern age of the majority of the ~~herein~~ studied sediments. This is further supported by AMS ^{14}C-dating of calcareous microfossils and ^{210}Pb-dating of seafloor surface sediments from the Amundsen Sea shelf documenting recent ages for most sites (Hillenbrand et al., 2010, 2013, 2017; Smith et al., 2011, 2014, 2017; Witus et al., 2014) as well as modern ^{210}Pb-dates obtained for three multicores collected in ~~the~~ Bransfield Strait (PS97/56, PS97/68, PS97/72; Vorrath et al., 2020~~), which are considered in this study, too.~~). AMS ^{14}C dates obtained for nearby seafloor surface ~~samples~~sediments in the vicinity of the South Shetland Islands and the Antarctic Sound revealed ages of 100 years and 142 years BP, respectively (Vorrath et al., 2019). As both uncorrected ages lie within the range of the modern marine reservoir effect (e.g. Gordon and Harkness, 1992), we ~~may~~ consider these two dates still ~~modern~~as recent. However, in an area that is significantly affected by rapid climate warming over the past decades and a regionally variable sea–ice coverage, the age uncertainties ~~associated with ^{14}C dating of calcareous material~~for at least ^{14}C dated samples may easily lead to an over- or underestimation of biomarker-based sea-ice cover and ocean ~~temperature estimates~~temperatures, respectively, which needs to be ~~considered~~taken into account for comparisons with instrumental data. ~~While the~~The utilization of (paleo) model data may alleviate the lack of age control for each seafloor sediment sample to some extent. Nevertheless, we ~~accordingly~~ recommend that for a robust calibration of *e.g.*~~.~~ PIPSO$_{25}$ values against satellite-derived sea-ice concentrations ~~(and this is not the aim of this study)~~ only surface sediment samples with a modern age confirmed by ^{210}Pb-dating are incorporated.


5.2    Production and preservation of biomarkers

Biomarkers ~~are considered~~have the potential to reveal the former occurrence of their ~~precursor organisms~~producers, which requires ~~a certain~~ knowledge of the source ~~specificity~~organisms. While there is general consensus on ~~e.g.~~ Thaumarchaeota being the major source for iso-GDGTs (Fietz et al., 2020 and references therein) ~~or~~and diatoms synthesizing HBIs (Volkman 2006), ~~this is not~~the ~~case for~~main source of brassicasterol, which is not only found in diatoms but also in ~~e.g.~~ dinoflagellates and

haptophytes (Volkman 2006~~).~~), remains unclear. Accordingly, the use of brassicasterol to determine the PIPSO$_{25}$ index may introduce uncertainties regarding the environmental information ~~pertinent to~~recorded by this phytoplankton biomarker. A further aspect concerns the different chemical structures of HBIs and sterols, which raises the risk of a selective degradation (see Belt, 2018 and Rontani et al., 2018; 2019 for detailed discussion) with potentially considerable effects on the PIPSO$_{25}$ index. Regarding the different ~~sectors of the~~areas investigated in our study ~~area~~, also spatially different microbial communities ~~as well as~~and varying depositional regimes, such as sedimentation rate, redox conditions and water depth, may lead to different degradation patterns~~, which~~. This means that variations in the biomarker concentrations between different ~~sectors~~areas may not strictly reflect changes in the production of these compounds (driven by sea surface conditions) but may also relate to different degradation states. In particular, lower sedimentation rates and thus extended oxygen exposure times promote chemical alteration and degradation processes (Hedges et al., 1990; Schouten et al., 2013). ~~Regarding the transport of organic matter from the sea surface through the water column~~However, it has been previously ~~noted~~reported that the formation of mineral aggregates and fecal pellets~~, however,~~ often accelerates the ~~vertical export towards~~transport of organic matter from the sea surface through the water column to the seafloor during the melting season~~,~~ leading to a more rapid burial and hence better preservation of the organic compounds (Bauerfeind et al., 2005; Etourneau et al., 2019; Müller et al., 2011).

Another rather technical drawback concerning the use of the PIPSO$_{25}$ index ~~may appear~~occurs when the concentrations of the sea-ice proxy IPSO$_{25}$ and the phytoplankton marker are similarly low (due to unfavourable conditions for both ice algae ~~as well as~~and phytoplankton) or similarly high (due to a significant seasonal shift in sea-ice cover and/or stable ice edge conditions). This may lead to similar PIPSO$_{25}$ values, although the sea-ice conditions are fundamentally different from each other. This scenario ~~occurred at~~is evident for five sampling sites in the Weddell Sea (PS111/13-2, /15-1, /16-3, /29-3, and /40-2; Fig. 3b+c), where IPSO$_{25}$ and the HBI Z-triene concentrations are close to the detection limit and P$_Z$IPSO$_{25}$ values are very low, suggesting a reduced sea-ice cover. Satellite and model data, however, show that these sample locations are influenced by heavy, nearly year-round sea-ice cover. We conclude that biomarker concentrations of both biomarkers at or close to the detection limit~~,~~

618 ~~indicative of a severe ice cover,~~ need to be treated with caution. ~~As mentioned above~~Here, we assigned

619 a maximum $P_Z IPSO_{25}$ value of 1 to ~~these~~those samples, and we note that such a practice always needs

620 to be ~~made clear~~clarified when applying the $PIPSO_{25}$ approach. ~~The~~Nonetheless, the coupling of $IPSO_{25}$

621 with a phytoplankton marker~~, nonetheless,~~ provides more reliable sea-ice reconstructions. Regarding

622 ~~the above-mentioned~~all these ambiguities, we recommend not only to calculate the $PIPSO_{25}$ index, but

623 also to carefully consider individual biomarker concentrations and, if possible, to utilize other sea-~~ice~~

624 ~~measures~~iceproxies, such as data from well-preserved diatom ~~assemblage data~~assemblages (Lamping

625 et al., 2020; Vorrath et al., 2019; 2020). While the $PIPSO_{25}$ index is not yet a fully quantitative proxy

626 ~~to provide~~for paleo sea-ice concentrations, ~~the GDGT paleothermometers have gone through~~ several

627 calibration iterations have been applied to the GDGT-paleothermometers (Fietz et al., 2020). As noted

628 above, the observation of distinctly warm-biased $TEX^L_{86}$-derived SOTs calls for further efforts ~~in terms~~

629 of regional calibration studies and/or investigations of archaean adaptation strategies ~~regarding~~at

630 different water depths~~,~~ and under different nutrient and temperature conditions.

631

632      5.3    The role of platelet ice for the production of $IPSO_{25}$

633 The sympagic, tube-dwelling, diatom *B. adeliensis* is a common constituent of Antarctic sea ice~~,~~ and

634 preferably ~~flourishing~~flourishes in the relatively open channels of sub-ice platelet layers in near-shore

635 locations covered by fast ice (Medlin, 1990; Riaux-Gobin and Poulin, 2004). Based on investigations

636 of sea-ice samples from the Southern Ocean, Belt et al. (2016) detected this diatom species to be a

637 source of $IPSO_{25}$, which, according to its habitat, led to the assumption of the sea-ice proxy being a

638 potential indicator for the presence of platelet ice. As stated above, *B. adeliensis* is not confined to

639 platelet ice, but is also observed in basal sea ice and described as well adapted to changes in the texture

640 of sea ice during ice melt (Riaux-Gobin et al., 2013). Platelet ice formation, however, plays an important

641 role in sea-ice generation along some coastal regions of Antarctica (Hoppmann et al., 2015; 2020; Lange

642 et al., 1989; Langhorne et al., 2015). In these regions, CDW and High Saline Shelf Water (HSSW)

643 ~~flowing~~flow into sub-ice shelf cavities of ice shelves and cause basal melting and the discharge of cold

644 and less saline water (Fig. 8; Hoppmann et al., 2020, Scambos et al., 2017). The surrounding water is

645 cooled and freshened and is then transported towards the surface. Under the large Filchner-Ronne and

646 Ross ice shelves the pressure relief can cause this water, called Ice Shelf Water (ISW), to be supercooled

647 (Foldvik and Kvinge, 1974). The temperature of the supercooled ISW is ~~potentially~~typically below the

648 in-situ freezing point, which ~~may~~ eventually ~~cause~~causes the formation of ice platelets that accumulate

649 under landfast ice attached to adjacent ice shelves (Fig. 8; Holland et al., 2007; Hoppmann et al., 2015;
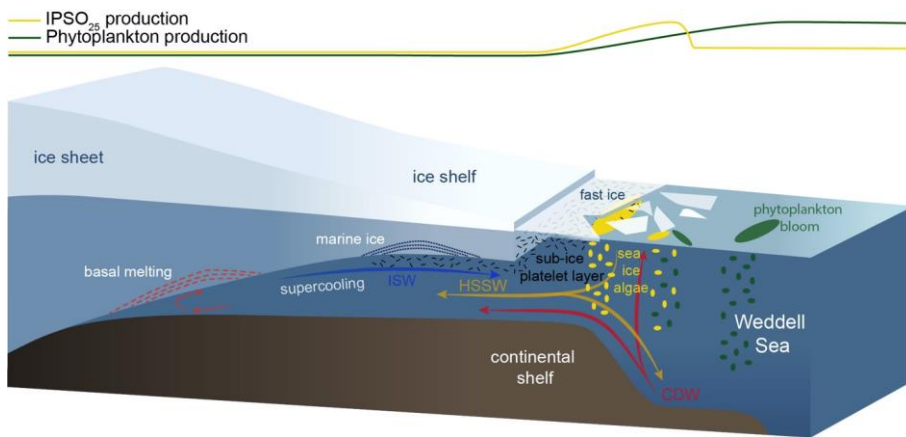
650 2020).



**Fig. 8:** Schematic illustration of the formation of platelet ice and the main production areas of sea ice algae producing IPSO$_{25}$ (yellow ~~ovals~~ellipses) and phytoplankton (green ~~ovals~~ellipses), also displayed by yellow and green curves at the top. CDW: Circumpolar Deep Water, HSSW: High Saline Shelf Water, ISW: Ice Shelf Water. ~~Schematic~~Illustration modified ~~after~~from Scambos et al. (2017).

651 In an attempt to elucidate the relationship ~~of~~between IPSO$_{25}$ and platelet ice ~~more clearly~~, we ~~here~~

652 ~~regard~~investigated our data in ~~connection~~respect to locations of observed platelet ~~ice occurrences.~~

653 iceformation. While the maximum IPSO$_{25}$ concentrations in front of the Filchner Ice Shelf could be

654 directly related to the above-mentioned platelet ice formation in this area, the elevated IPSO$_{25}$

655 concentrations ~~in front~~north of the Larsen C Ice ~~Shelves~~Shelf at the EAP could be linked to several

656 processes. According to Langhorne et al. (2015), sea-ice cores retrieved from that area did not

657 incorporate platelet ice. The high IPSO$_{25}$ concentrations could hence be ~~explicable~~explained by either

658 input from drift ice transported with the Weddell Gyre or by basal freeze-on. ~~We do, however,~~However,

659 we note that our samples may reflect much longer time ~~frames~~periods than the sea-ice samples

660 investigated by Langhorne et al. (2015) and the lack of platelet ice in their investigated sea-ice cores

661  does not rule out the former presence of platelet ice, which may be captured in our investigated sediment

662  samples.

663  There are several previous studies on IPSO$_{25}$ ~~which report~~that reported a close connection of the proxy

664  ~~to~~with proximal, coastal locations and polynyas in the seasonal ice zone (*i.e.*,, Collins et al., 2013; Smik

665  et al., 2016). They do not, however, discuss the relation to adjacent ice shelves as possible "platelet ice

666  factories". We note that the core locations investigated by Smik et al. (2016) are in the vicinity of the

667  Moscow University Ice Shelf, where Langhorne et al. (2015), did not observe platelet ice within sea-ice

668  cores. Hoppmann et al. (2020), however, report a sea-ice core from that area, which incorporates platelet

669  ice. The different observations by Langhorne et al. (2015) and Hoppmann et al. (2020) highlight the

670  temporal variability in the occurrence of platelet ice in the cold water regime around the East Antarctic

671  margin.

672  ~~Regarding~~For the observed IPSO$_{25}$ minimum ~~abundance of IPSO$_{25}$~~ in the Amundsen Sea (Fig. 3b; AS),

673  which we tentatively relate to the extended and thick sea--ice coverage, the absence of platelet ice ~~in~~

674  ~~that region may be~~there is an alternative explanation. The Amundsen/Bellingshausen Sea and WAP

675  shelves are classified as "warm shelves" (Thompson et al., 2018~~) characterized by~~), where the

676  upwelling of warm CDW (Schmidtko et al., 2014~~), hindering~~) hinders the formation of ISW ~~and~~

677  ~~making,~~ which makes the presence of platelet ice ~~in~~under recent conditions highly unlikely (Hoppmann

678  et al., 2020). This ~~theory~~ is also supported by Langhorne et al. (2015), ~~stating~~who stated that platelet

679  ice formation is not observed, in areas where ~~thinning from~~ basal ice-shelf melting ~~of ice shelves is~~

680  ~~believed to be greatest, which applies to~~is considerable, such as on the ~~warm~~ West Antarctic continental

681  shelf in the eastern Pacific sector of the Southern Ocean (Thompson et al., 2018). Accordingly, if the

682  formation and accumulation of platelet ice – up to a certain degree  – ~~is indicative of basal~~indicates sub-

683  ice shelf melting on ~~fresh~~"cold shelves" (Hoppmann et al., 2015; Thompson et al., 2018), high IPSO$_{25}$

684  concentrations ~~determined~~found in marine sediments may hence serve as indicator of past ISW

685  formation and associated ice shelf dynamics. ~~This may~~This is, however, probably only ~~be~~true up to a

686  certain threshold, where platelet ice formation decreases or is ~~diminished/~~hampered due to warm

687  oceanic conditions causing too intense sub-ice shelf melting (Langhorne et al., 2015).

688  ~~While~~When using IPSO$_{25}$ as a sea-ice proxy in Antarctica, it is ~~hence~~ important to ~~also~~ consider regional

689  platelet ice formation processes ~~as~~, too, because these may affect the IPSO$_{25}$ budget. Determining

690  thresholds associated with platelet ice formation is challenging. Therefore, further investigations, such

691  as in-situ measurements of IPSO$_{25}$ concentrations in platelet ice or culture experiments in ~~home~~

692  laboratories, are needed to better ~~depict~~understand the connection between IPSO$_{25}$ and platelet ice

693  formation (and basal ice-~~shelf basal~~ shelf melting).

694

695  **7. Conclusions**

696  Biomarker analyses focusing on IPSO$_{25}$, HBI-trienes, phytosterols and GDGTs in surface sediment

697  samples from the Antarctic continental margin were investigated to depict recent sea-ice conditions

698  and ocean temperatures in this climate sensitive region. Proxy-based reconstructions of these key

699  variables were compared to (1) satellite sea-ice data, (2) instrumental ocean temperature data ~~as well~~

700  ~~as,~~ and (3) modelled sea-ice patterns and ocean temperatures. The semi-quantitative sea-ice index

701  PIPSO$_{25}$, combining the sea-ice proxy IPSO$_{25}$ with an open-water phytoplankton marker, yielded

702  reasonably good correlations with satellite observations and numerical model results, while correlations

703  with the sea-ice proxy IPSO$_{25}$ alone are rather low. Minimum concentrations of both biomarkers, used

704  for the PIPSO$_{25}$ calculations, ~~however,~~ may lead to ambiguous interpretations and significant

705  underestimations of sea-ice conditions. ~~Different~~Therefore, different sea-ice measures should be

706  considered when interpreting biomarker data ~~should hence be considered~~.

707  Ocean temperature reconstructions based on the TEX$^{L}_{86}$ and RI-OH'-paleothermometers show similar

708  patterns, but different absolute temperatures. While TEX$^{L}_{86}$-derived temperatures are significantly

709  biased towards warm temperatures in Drake Passage, the RI-OH'-derived temperature range seems

710  more realistic~~,~~ when compared to temperature data based on the WOA13 and modelled annual mean

711  SOTs.

712  Further investigations of HBI- as well as GDGT-synthesis, transport, ~~sedimentation~~deposition and

713  preservation within the sediments would help to guide the proxies' application. Further work on the

714  taxonomy ~~work~~of the IPSO$_{25}$ producers, the composition of ~~the IPSO$_{25}$ producer's~~their habitat (basal

715  sea ice, platelet ice, brine channels) and its connection to platelet ice formation via in-situ or laboratory

measurements are required to better constrain the $IPSO_{25}$ potential as a robust sea-ice biomarker. The presumed relationship between $IPSO_{25}$ and platelet ice formation in connection to sub-ice shelf melting is supported by our data, showing high $IPSO_{25}$ concentrations in areas with known platelet ice formation and low $IPSO_{25}$ concentrations in areas without observed platelet ice formation. Accordingly, oceanic conditions and the intensity of sub-ice shelf melting need to be considered when using $IPSO_{25}$ (1) as an indirect indicator for sub-ice shelf melting processes and associated ice shelf dynamics and (2) for the application of the $PIPSO_{25}$ index to estimate sea-ice coverage.

**Data availability**

Datasets related to this article can be found online on *PANGAEA Data Publisher for Earth & Environmental Science* (doi: in prep).

**Author contribution**

N.L. and J.M. designed the concept of the study. N.L. carried out biomarker experiments. X.S and G.L. developed the model code and X.S. performed the simulations. C.H. provided the satellite data. M.-E.V. provided hitherto unpublished GDGT data for PS97 samples. G.M. and J.H. carried out GDGT analyses. C.-D.H. collected surface sediment samples and advised on their ages. N.L. prepared the manuscript and visualizations with contributions from all co-authors.

**Competing interests**

The authors declare that they have no conflict of interest.

33

748

749 **References**

750 Abernathey, R. P., Cerovecki, I., Holland, P. R., Newsom, E., Mazloff, M., and Talley, L. D.: Water-

751 mass transformation by sea ice in the upper branch of the Southern Ocean overturning, Nature

752 Geoscience, 9, 596-601, 2016.

753 Allen, C. S., Pike, J., and Pudsey, C. J.: Last glacial–interglacial sea-ice cover in the SW Atlantic

754 and its potential role in global deglaciation, Quaternary Science Reviews, 30, 2446-2458, 2011.

755 Alonso-Sáez, L., Andersson, A., Heinrich, F., and Bertilsson, S.: High archaeal diversity in Antarctic

756 circumpolar deep waters, Environmental microbiology reports, 3, 689-697, 2011.

757 Anderson, P. S.: Evidence for an Antarctic winter coastal polynya, Antarctic science, 5, 221-226,

758 1993.

759 Armand, L. K., and Leventer, A.: Palaeo sea ice distribution–reconstruction and palaeoclimatic

760 significance, Sea ice—an introduction to its physics, biology, chemistry, and geology, 333-372,

761 2003.

762 Arrigo, K. R., Worthen, D. L., Lizotte, M. P., Dixon, P., and Dieckmann, G.: Primary production in

763 Antarctic sea ice, Science, 276, 394-397, 1997.

764 Arrigo, K. R.: Sea ice as a habitat for primary producers, Sea ice, 352-369, 2017.

765 Barbara, L., Crosta, X., Massé, G., and Ther, O.: Deglacial environments in eastern Prydz Bay, East

766 Antarctica, Quaternary Science Reviews, 29, 2731-2740, 2010.

767 Barbara, L., Crosta, X., Schmidt, S., and Massé, G.: Diatoms and biomarkers evidence for major

768 changes in sea ice conditions prior the instrumental period in Antarctic Peninsula, Quaternary

769 Science Reviews, 79, 99-110, 2013.

Kommentiert [NL1]: I will double-check the reference-list before submission.

Bauerfeind, E., Leipe, T. and Ramseier, R.O.: Sedimentation at the permanently ice-covered Greenland continental shelf (74°57.7'N/12°58.7'W): significance of biogenic and lithogenic particles in particulate matter flux. Journal of Marine Systems 56, 151-166, 2005.

Belt, S. T., Allard, W. G., Massé, G., Robert, J.-M., and Rowland, S. J.: Highly branched isoprenoids (HBIs): identification of the most common and abundant sedimentary isomers, Geochimica et Cosmochimica Acta, 64, 3839-3851, 2000.

Belt, S. T., and Müller, J.: The Arctic sea ice biomarker $IP_{25}$: a review of current understanding, recommendations for future research and applications in palaeo sea ice reconstructions, Quaternary Science Reviews, 79, 9-25, 2013.

Belt, S. T., Brown, T. A., Ampel, L., Cabedo-Sanz, P., Fahl, K., Kocis, J. J., Masse, G., Navarro-Rodriguez, A., Ruan, J., and Xu, Y.: An inter-laboratory investigation of the Arctic sea ice biomarker proxy $IP_{25}$ in marine sediments: key outcomes and recommendations, Climate of the Past., 10, 155-166, 2014.

Belt, S. T., Cabedo-Sanz, P., Smik, L., Navarro-Rodriguez, A., Berben, S. M. P., Knies, J., and Husum, K.: Identification of paleo Arctic winter sea ice limits and the marginal ice zone: Optimised biomarker-based reconstructions of late Quaternary Arctic sea ice, Earth and Planetary Science Letters, 431, 127-139, 2015.

Belt, S. T., Smik, L., Brown, T. A., Kim, J. H., Rowland, S. J., Allen, C. S., Gal, J. K., Shin, K. H., Lee, J. I., and Taylor, K. W. R.: Source identification and distribution reveals the potential of the geochemical Antarctic sea ice proxy $IPSO_{25}$, Nature Communications, 7, 12655, https://doi.org/10.1038/ncomms12655, 2016.

Belt, S. T., Brown, T. A., Smik, L., Tatarek, A., Wiktor, J., Stowasser, G., Assmy, P., Allen, C. S., and Husum, K.: Identification of $C_{25}$ highly branched isoprenoid (HBI) alkenes in diatoms of the genus Rhizosolenia in polar and sub-polar marine phytoplankton, Organic Geochemistry, 110, 65-72, 2017.

Belt, S. T.: Source-specific biomarkers as proxies for Arctic and Antarctic sea ice, Organic Geochemistry, 125, 277-298, 2018.

797 Berger, A.: Long-term variations of daily insolation and Quaternary climatic changes, Journal of the
798     atmospheric sciences, 35, 2362-2367, 1978.

799 Blain, S., Quéguiner, B., Armand, L., Belviso, S., Bombled, B., Bopp, L., Bowie, A., Brunet, C.,
800     Brussaard, C., Carlotti, F., Christaki, U., Corbière, A., Durand, I., Ebersbach, F., Fuda, J.-L.,
801     Garcia, N., Gerringa, L., Griffiths, B., Guigue, C., Guillerm, C., Jacquet, S., Jeandel, C., Laan,
802     P., Lefèvre, D., Lo Monaco, C., Malits, A., Mosseri, J., Obernosterer, I., Park, Y.-H., Picheral,
803     M., Pondaven, P., Remenyi, T., Sandroni, V., Sarthou, G., Savoye, N., Scouarnec, L., Souhaut,
804     M., Thuiller, D., Timmermans, K., Trull, T., Uitz, J., van Beek, P., Veldhuis, M., Vincent, D.,
805     Viollier, E., Vong, L. and Wagener, T.: Effect of natural iron fertilization on carbon sequestration
806     in the Southern Ocean. Nature 446, 1070-1074, 2007.

807 Boon, J. J., Rijpstra, W. I. C., de Lange, F., De Leeuw, J., Yoshioka, M., and Shimizu, Y.: Black
808     Sea sterol—a molecular fossil for dinoflagellate blooms, Nature, 277, 125-127, 1979.

809 Cavalieri, D., Parkinson, C., Gloersen, P., and Zwally, H.: Sea ice concentrations from Nimbus-7
810     SMMR and DMSP SSM/I passive microwave data, National Snow and Ice Data Center, Boulder,
811     Colorado, USA, 1996.

812 Collares, L. L., Mata, M. M., Kerr, R., Arigony-Neto, J., and Barbat, M. M.: Iceberg drift and ocean
813     circulation in the northwestern Weddell Sea, Antarctica, Deep Sea Research Part II: Topical
814     Studies in Oceanography, 149, 10-24, 2018.

815 Colleoni, F., De Santis, L., Siddoway, C. S., Bergamasco, A., Golledge, N. R., Lohmann, G.,
816     Passchier, S., and Siegert, M. J.: Spatio-temporal variability of processes across Antarctic ice-
817     bed–ocean interfaces, Nature Communications, 9, 2289, https://doi.org/10.1038/s41467-018-
818     04583-0, 2018.

819 Collins, L. G., Allen, C. S., Pike, J., Hodgson, D. A., Weckström, K., and Massé, G.: Evaluating
820     highly branched isoprenoid (HBI) biomarkers as a novel Antarctic sea-ice proxy in deep ocean
821     glacial age sediments, Quaternary Science Reviews, 79, 87-98, 2013.

822 Comiso, J. C., Gersten, R. A., Stock, L. V., Turner, J., Perez, G. J., and Cho, K.: Positive Trend in
823     the Antarctic Sea Ice Cover and Associated Changes in Surface Temperature, Journal of Climate,
824     30, 2251-2267, 2017.

825    Cook, A.J., Holland, P., Meredith, M., Murray, T., Luckman, A., Vaughan, D.G.: Ocean forcing of
826        glacier retreat in the WAP. Science, 353, 283-286, 2016.

827    Crosta, X., Pichon, J. J., and Burckle, L.: Application of modern analog technique to marine
828        Antarctic diatoms: Reconstruction of maximum sea-ice extent at the Last Glacial Maximum,
829        Paleoceanography and Paleoclimatology, 13, 284-297, 1998.

830    Crosta, X., Etourneau, J., Orme, L.C., Dalaiden, Q., Campagne, P., Swingedouw, D., Goosse, H.,
831        Massé, G., Miettinen, A., McKay, R.M., Dunbar, R.B., Escutia, C. and Ikehara, M.: Multi-
832        decadal trends in Antarctic sea-ice extent driven by ENSO–SAM over the last 2,000 years. Nature
833        Geoscience 14, 156-160, 2021.

834    Danilov, S., Sidorenko, D., Wang, Q., and Jung, T.: The Finite-volumE Sea ice–Ocean Model
835        (FESOM2), Geosci. Model Dev., 10, 765-789, 2017.de Jong, J., Schoemann, V., Lannuzel, D.,
836        Croot, P., de Baar, H. and Tison, J.-L.: Natural iron fertilization of the Atlantic sector of the
837        Southern Ocean by continental shelf sources of the Antarctic Peninsula. Journal of Geophysical
838        Research: Biogeosciences 117, 2012.

839    Denis, D., Crosta, X., Barbara, L., Massé, G., Renssen, H., Ther, O., and Giraudeau, J.: Sea ice and
840        wind variability during the Holocene in East Antarctica: insight on middle–high latitude coupling,
841        Quaternary Science Reviews, 29, 3709-3719, 2010.

842    Dorschel, B.: The Expedition PS118 of the Research Vessel POLARSTERN to the Weddell Sea in
843        2019, Berichte zur Polar-und Meeresforschung = Reports on polar and marine research, 735,
844        2019.

845    Doty, M. S., and Oguri, M.: The island mass effect, ICES Journal of Marine Science, 22, 33-37,
846        1956.

847    Eayrs, C., Li, X., Raphael, M.N. and Holland, D.M.: Rapid decline in Antarctic sea ice in recent
848        years hints at future change. Nature Geoscience 14, 460-464, 2021.

849    Esper, O., and Gersonde, R.: New tools for the reconstruction of Pleistocene Antarctic sea ice,
850        Palaeogeography, Palaeoclimatology, Palaeoecology, 399, 260-283, 2014.

851    Etourneau, J., Collins, L. G., Willmott, V., Kim, J.-H., Barbara, L., Leventer, A., Schouten, S.,
852        Damsté, J. S., Bianchini, A., and Klein, V.: Holocene climate variations in the WAP: evidence

853     for sea ice extent predominantly controlled by changes in insolation and ENSO variability,
854     Climate of the Past, 9, 1431-1446, 2013.

855 Etourneau, J., Sgubin, G., Crosta, X., Swingedouw, D., Willmott, V., Barbara, L., Houssais, M.-N.,
856     Schouten, S., Damsté, J.S.S., Goosse, H.: Ocean temperature impact on ice shelf extent in the
857     eastern Antarctic Peninsula. Nature Communications 10, 1-8, 2019.

858 Fahl, K., and Stein, R.: Modern seasonal variability and deglacial/Holocene change of central Arctic
859     Ocean sea-ice cover: new insights from biomarker proxy records, Earth and Planetary Science
860     Letters, 351, 123-133, 2012.

861  Fetterer, F., Knowles, K., Meier, W., Savoie, M., Windnagel, A.K., 2016. Updated Daily. Sea Ice
862     Index, Version 2. [Median Sea Ice Extent 1981-2010]. NSIDC: National Snow and Ice Data
863     Center, Boulder, Colorado USA. https://doi.org/10.7265/N5736NV7 [24 July 2017].

864 Fietz, S., Huguet, C., Rueda, G., Hambach, B., and Rosell-Melé, A.: Hydroxylated isoprenoidal
865     GDGTs in the Nordic Seas, Marine Chemistry, 152, 1-10, 2013.

866 Fietz, S., Ho, S., and Huguet, C.: Archaeal Membrane Lipid-Based Paleothermometry for
867     Applications in Polar Oceans, Oceanography, 33, 104-114, 2020.

868 Foldvik, A., and Kvinge, T.: Conditional instability of sea water at the freezing point, Deep Sea
869     Research and Oceanographic Abstracts, 21, 169-174, 1974.

870 Fretwell, P., Pritchard, H.D., Vaughan, D.G., 57 others. Bedmap2: improved ice bed, surface and
871     thickness datasets for Antarctica. Cryosphere 7, 375-393. http://dx.doi.org/10.5194/tc-7-375-
872     2013, 2013.

873 Gersonde, R., and Zielinski, U.: The reconstruction of late Quaternary Antarctic sea-ice
874     distribution—the use of diatoms as a proxy for sea-ice, Palaeogeography, Palaeoclimatology,
875     Palaeoecology, 162, 263-286, 2000.

876 Gohl, K.: The expedition ANTARKTIS-XXIII/4 of the research vessel Polarstern in 2006, Berichte
877     zur Polar-und Meeresforschung (Reports on Polar and Marine Research), 557, 2007.

878 Gohl, K.: The Expedition PS104 of the Research Vessel POLARSTERN to the Amundsen Sea in
879     2017, Berichte zur Polar-und Meeresforschung = Reports on polar and marine research, 712,
880     2017.

881    Gordon, J.E., Harkness, D.D.: Magnitude and geographic variation of the radiocarbon content in

882        Antarctic marine life: implications for reservoir corrections in radiocarbon dating, Quaternary

883        Science Reviews 11, 697-708, 1992.

884    Hancke, K., Lund-Hansen, L. C., Lamare, M. L., Højlund Pedersen, S., King, M. D., Andersen, P.,

885        and Sorrell, B. K.: Extreme low light requirement for algae growth underneath sea ice: A case

886        study from Station Nord, NE Greenland, Journal of Geophysical Research: Oceans, 123, 985-

887        1000, 2018.

888    Harms, S., Fahrbach, E., and Strass, V. H.: Sea ice transports in the Weddell Sea, Journal of

889        Geophysical Research: Oceans, 106, 9057-9073, 2001.

890    Hedges, J.I., Hu, F.S., Devol, A.H., Hartnett, H.E., Tsamakis, E. and Keil, R.G.: Sedimentary organic

891        matter preservation; a test for selective degradation under oxic conditions. Am J Sci 299, 529-

892        555, 1999.

893    Hellmer, H.H., Rhein, M., Heinemann, G., Abalichin, J., Abouchami, W., Baars, O., Cubasch, U.,

894        Dethloff, K., Ebner, L., Fahrbach, E., Frank, M., Gollan, G., Greatbatch, R.J., Grieger, J.,

895        Gryanik, V.M., Gryschka, M., Hauck, J., Hoppema, M., Huhn, O., Kanzow, T., Koch, B.P.,

896        König-Langlo, G., Langematz, U., Leckebusch, G.C., Lüpkes, C., Paul, S., Rinke, A., Rost, B.,

897        van der Loeff, M.R., Schröder, M., Seckmeyer, G., Stichel, T., Strass, V., Timmermann, R.,

898        Trimborn, S., Ulbrich, U., Venchiarutti, C., Wacker, U., Willmes, S. and Wolf-Gladrow, D.:

899        Meteorology and oceanography of the Atlantic sector of the Southern Ocean - a review of German

900        achievements from the last decade. Ocean Dynamics 66, 1379-1413, 2016.

901    Hillenbrand, C.-D., Smith, J.A., Kuhn, G., Esper, O., Gersonde, R., Larter, R.D., Maher, B.,

902        Moreton, S.G., Shimmield, T.M., Korte, M.: Age assignment of a diatomaceous ooze deposited

903        in the western Amundsen Sea Embayment after the Last Glacial Maximum. Journal of

904        Quaternary Science 25, 280-295, 2010.

905    Hillenbrand, C.-D., Kuhn, G., Smith, J.A., Gohl, K., Graham, A.G.C., Larter, R.D., Klages, J.P.,

906        Downey, R., Moreton, S.G., Forwick, M., Vaughan, D.G.: Grounding-line retreat of the West

907        Antarctic Ice Sheet from inner Pine Island Bay. Geology 41, 35-38, 2013.

908     Hillenbrand, C.-D., Smith, J.A., Hodell, D.A., Greaves, M., Poole, C.R., Kender, S., Williams, M.,

909           Andersen, T.J., Jernas, P.E., Elderfield, H., Klages, J.P., Roberts, S.J., Gohl, K., Larter, R.D.,

910           Kuhn, G.: West Antarctic Ice Sheet retreat driven by Holocene warm water intrusions. Nature

911           547, 43–48, 2017.

912     Ho, S. L., Mollenhauer, G., Fietz, S., Martínez-Garcia, A., Lamy, F., Rueda, G., Schipper, K.,

913           Méheust, M., Rosell-Melé, A., Stein, R., and Tiedemann, R.: Appraisal of $TEX_{86}$ and

914           thermometries in subpolar and polar regions, Geochimica et Cosmochimica Acta, 131, 213-226,

915           2014.

916     Hobbs, W. R., Massom, R., Stammerjohn, S., Reid, P., Williams, G., and Meier, W.: A review of

917           recent changes in Southern Ocean sea ice, their drivers and forcings, Global and Planetary

918           Change, 143, 228-250, 2016.

919     Holland, P. R., Feltham, D. L., and Jenkins, A.: Ice shelf water plume flow beneath Filchner-Ronne

920           Ice Shelf, Antarctica, Journal of Geophysical Research: Oceans, 112,

921           https://doi.org/10.1029/2006JC003915, 2007.

922     Hopmans, E. C., Weijers, J. W., Schefuß, E., Herfort, L., Damsté, J. S. S., and Schouten, S.: A novel

923           proxy for terrestrial organic matter in sediments based on branched and isoprenoid tetraether

924           lipids, Earth and Planetary Science Letters, 224, 107-116, 2004.

925     Hoppmann, M., Nicolaus, M., Paul, S., Hunkeler, P. A., Heinemann, G., Willmes, S., Timmermann,

926           R., Boebel, O., Schmidt, T., and Kühnel, M.: Ice platelets below Weddell Sea landfast sea ice,

927           Annals of Glaciology, 56, 175-190, 2015.

928     Hoppmann, M., Richter, M. E., Smith, I. J., Jendersie, S., Langhorne, P. J., Thomas, D. N., and

929           Dieckmann, G. S.: Platelet ice, the Southern Ocean's hidden ice: a review, Annals of Glaciology,

930           1-28, 2020.

931     Huguet, C., de Lange, G. J., Gustafsson, Ö., Middelburg, J. J., Damsté, J. S. S., and Schouten, S.:

932           Selective preservation of soil organic matter in oxidized marine sediments (Madeira Abyssal

933           Plain), Geochimica et Cosmochimica Acta, 72, 6061-6068, 2008.

934     Iacono, M. J., Delamere, J. S., Mlawer, E. J., Shephard, M. W., Clough, S. A., and Collins, W. D.:

935           Radiative forcing by long-lived greenhouse gases: Calculations with the AER radiative transfer

936     models, Journal of Geophysical Research: Atmospheres, 113,
937          https://doi.org/10.1029/2008JD009944, 2008.

938  Jacobs, S. S., Jenkins, A., Giulivi, C. F., and Dutrieux, P.: Stronger ocean circulation and increased
939          melting under Pine Island Glacier ice shelf, Nature Geoscience, 4, 519-523, 2011.

940  Jenkins, A., and Jacobs, S.: Circulation and melting beneath George VI ice shelf, Antarctica, Journal
941          of Geophysical Research: Oceans, 113, https://doi.org/10.1029/2007JC004449, 2008.

942  Johns, L., Wraige, E., Belt, S., Lewis, C., Massé, G., Robert, J.-M., and Rowland, S.: Identification
943          of a $C_{25}$ highly branched isoprenoid (HBI) diene in Antarctic sediments, Antarctic sea-ice diatoms
944          and cultured diatoms, Organic Geochemistry, 30, 1471-1475, 1999.

945  Kalanetra, K. M., Bano, N., and Hollibaugh, J. T.: Ammonia-oxidizing Archaea in the Arctic Ocean
946          and Antarctic coastal waters, Environmental Microbiology, 11, 2434-2445, 2009.

947  Khazendar, A., Rignot, E., Schroeder, D.M., Seroussi, H., Schodlok, M.P., Scheuchl, B., Mouginot,
948          J., Sutterley, T.C., Velicogna, I.: Rapid submarine ice melting in the grounding zones of ice
949          shelves in West Antarctica. Nature communications 7, 1-8, 2016.

950  Kim, J.-H., Van der Meer, J., Schouten, S., Helmke, P., Willmott, V., Sangiorgi, F., Koç, N.,
951          Hopmans, E. C., and Damsté, J. S. S.: New indices and calibrations derived from the distribution
952          of crenarchaeal isoprenoid tetraether lipids: Implications for past sea surface temperature
953          reconstructions, Geochimica et Cosmochimica Acta, 74, 4639-4654, 2010.

954  Kim, J.-H., Crosta, X., Willmott, V., Renssen, H., Bonnin, J., Helmke, P., Schouten, S., and
955          Sinninghe Damsté, J. S.: Holocene subsurface temperature variability in the eastern Antarctic
956          continental margin, Geophysical Research Letters, 39, https://doi.org/10.1029/2012GL051157,
957          2012.

958  Klinck, J. M., Hofmann, E. E., Beardsley, R. C., Salihoglu, B., and Howard, S.: Water-mass
959          properties and circulation on the WAP Continental Shelf in Austral Fall and Winter 2001, Deep
960          Sea Research Part II: Topical Studies in Oceanography, 51, 1925-1946, 2004.

961  Köhler, P., Nehrbass-Ahles, C., Schmitt, J., Stocker, T. F., and Fischer, H.: A 156 kyr smoothed
962          history of the atmospheric greenhouse gases $CO_2$, $CH_4$, and $N_2O$ and their radiative forcing, Earth
963          Syst. Sci. Data, 9, 363-387, 2017.

964     Lamping, N., Müller, J., Esper, O., Hillenbrand, C.-D., Smith, J. A., and Kuhn, G.: Highly branched
965         isoprenoids reveal onset of deglaciation followed by dynamic sea-ice conditions in the western
966         Amundsen Sea, Antarctica, Quaternary Science Reviews, 228,
967         https://doi.org/10.1016/j.quascirev.2019.106103, 2020.

968     Lange, M., Ackley, S., Wadhams, P., Dieckmann, G., and Eicken, H.: Development of sea ice in the
969         Weddell Sea, Annals of Glaciology, 12, 92-96, 1989.

970     Langhorne, P., Hughes, K., Gough, A., Smith, I., Williams, M., Robinson, N., Stevens, C., Rack,
971         W., Price, D., and Leonard, G.: Observed platelet ice distributions in Antarctic sea ice: An index
972         for ocean-ice shelf heat flux, Geophysical Research Letters, 42, 5442-5451, 2015.

973     Leventer, A.: The fate of Antarctic "sea ice diatoms" and their use as paleoenvironmental indicators,
974         Antarctic sea ice. Biological processes, interactions and variability, 121-137, 1998.

975     Li, X., Holland, D.M., Gerber, E.P. and Yoo, C.:Impacts of the north and tropical Atlantic Ocean on
976         the Antarctic Peninsula and sea ice. Nature 505, 538-542, 2014.

977     Liu, J., Curry, J. A., and Martinson, D. G.: Interpretation of recent Antarctic sea ice variability,
978         Geophysical Research Letters, 31, https://doi.org/10.1029/2003GL018732, 2004.

979     Liu, R., Han, Z., Zhao, J., Zhang, H., Li, D., Ren, J., Pan, J., Zhang, H.: Distribution and source of
980         glycerol dialkyl glycerol tetraethers (GDGTs) and the applicability of GDGT-based temperature
981         proxies in surface sediments of Prydz Bay, East Antarctica. Polar Research, 2020.

982     Locarnini, R. A., Mishonov, A. V., Antonov, J. I., Boyer, T. P., Garcia, H. E., Baranova, O. K.,
983         Zweng, M. M., Paver, C. R., Reagan, J. R., and Johnson, D. R.: World ocean atlas 2013. Volume
984         1, Temperature, NOAA Atlas NESDIS 73, 40 pp., doi: 10.7289/V55X26VD, 2013.

985     Lohmann, G., Butzin, M., Eissner, N., Shi, X., and Stepanek, C.: Abrupt climate and weather
986         changes across time scales, Paleoceanography and Paleoclimatology, 35,
987         https://doi.org/10.1029/2019PA003782, 2020.

988     López-García, P., Rodriguez-Valera, F., Pedrós-Alió, C., and Moreira, D.: Unexpected diversity of
989         small eukaryotes in deep-sea Antarctic plankton, Nature, 409, 603-607, 2001.

990     Lorenz, S. J., and Lohmann, G.: Acceleration technique for Milankovitch type forcing in a coupled

991         atmosphere-ocean circulation model: method and application for the Holocene, Climate

992         Dynamics, 23, 727-743, 2004.

993     Lott, F.: Alleviation of stationary biases in a GCM through a mountain drag parameterization scheme

994         and a simple representation of mountain lift forces, Monthly weather review, 127, 788-801, 1999.

995     Loveland, T. R., Reed, B. C., Brown, J. F., Ohlen, D. O., Zhu, Z., Yang, L., and Merchant, J. W.:

996         Development of a global land cover characteristics database and IGBP DISCover from 1 km

997         AVHRR data, Int. J. Remote Sens., 21, 1303-1330, 2000.

998     Lü, X., Liu, X.-L., Elling, F. J., Yang, H., Xie, S., Song, J., Li, X., Yuan, H., Li, N., and Hinrichs,

999         K.-U.: Hydroxylated isoprenoid GDGTs in Chinese coastal seas and their potential as a

1000        paleotemperature proxy for mid-to-low latitude marginal seas, Organic Geochemistry, 89-90, 31-

1001        43, 2015.

1002    Massé, G., Belt, S. T., Crosta, X., Schmidt, S., Snape, I., Thomas, D. N., and Rowland, S. J.: Highly

1003        branched isoprenoids as proxies for variable sea ice conditions in the Southern Ocean, Antarctic

1004        Science, 23, 487-498, 2011.

1005    Massom, R. A., Scambos, T. A., Bennetts, L. G., Reid, P., Squire, V. A., and Stammerjohn, S. E.:

1006        Antarctic ice shelf disintegration triggered by sea ice loss and ocean swell, Nature, 558, 383-389,

1007        2018.

1008    Medlin, L.: Berkeleya spp. from Antarctic waters, including Berkeleya adeliensis, sp. nov., a new

1009        tube dwelling diatom from the undersurface of sea-ice, Beihefte zur Nova Hedwigia, 100, 77-89,

1010        1990.

1011    Meredith, M. P., Woodworth, P. L., Chereskin, T. K., Marshall, D. P., Allison, L. C., Bigg, G. R.,

1012        Donohue, K., Heywood, K. J., Hughes, C. W., and Hibbert, A.: Sustained monitoring of the

1013        Southern Ocean at Drake Passage: Past achievements and future priorities, Reviews of

1014        Geophysics, 49, https://doi.org/10.1029/2010RG000348, 2011.

1015    Meyers, P. A.: Organic geochemical proxies of paleoceanographic, paleolimnologic, and

1016        paleoclimatic processes, Organic geochemistry, 27, 213-250, 1997.

1017    Moore, J. K., and Abbott, M. R.: Surface chlorophyll concentrations in relation to the Antarctic Polar

1018        Front: seasonal and spatial patterns from satellite observations, Journal of Marine Systems, 37,

1019        69-86, 2002.

1020    Müller, J., Wagner, A., Fahl, K., Stein, R., Prange, M., and Lohmann, G.: Towards quantitative sea

1021        ice reconstructions in the northern North Atlantic: A combined biomarker and numerical

1022        modelling approach, Earth and Planetary Science Letters, 306, 137-148, 2011.

1023    Müller, J., and Stein, R.: High-resolution record of late glacial and deglacial sea ice changes in Fram

1024        Strait corroborates ice–ocean interactions during abrupt climate shifts, Earth and Planetary

1025        Science Letters, 403, 446-455, 2014.

1026    Nakayama, Y., Schröder, M., Hellmer, H.H.: From circumpolar deep water to the glacial meltwater

1027        plume on the eastern Amundsen Shelf. Deep Sea Research Part I: Oceanographic Research

1028        Papers 77, 50-62, 2013.

1029    Nakayama, Y., Menemenlis, D., Zhang, H., Schodlok, M. and Rignot, E.: Origin of Circumpolar

1030        Deep Water intruding onto the Amundsen and Bellingshausen Sea continental shelves. Nature

1031        Communications 9, 3403, 2018.

1032    Nicholls, K. W., Østerhus, S., Makinson, K., Gammelsrød, T., and Fahrbach, E.: Ice-ocean processes

1033        over the continental shelf of the southern Weddell Sea, Antarctica: A review, Reviews of

1034        Geophysics, 47, https://doi.org/10.1029/2007RG000250, 2009.

1035    Nichols, P. D., Palmisano, A. C., Volkman, J. K., Smith, G. A., and White, D. C.: Occurrence of an

1036        isoprenoid $C_{25}$ diunasaturated alkene and high neutral lipid content in Antarctic sea-ice diatom

1037        communities 1, Journal of Phycology, 24, 90-96, 1988.

1038    Nielsdóttir, M. C., Bibby, T. S., Moore, C. M., Hinz, D. J., Sanders, R., Whitehouse, M., Korb, R.,

1039        and Achterberg, E. P.: Seasonal and spatial dynamics of iron availability in the Scotia Sea, Marine

1040        Chemistry, 130, 62-72, 2012.

1041    Nolting, R., De Baar, H., Van Bennekom, A., and Masson, A.: Cadmium, copper and iron in the

1042        Scotia Sea, Weddell Sea and Weddell/Scotia confluence (Antarctica), Marine Chemistry, 35,

1043        219-243, 1991.

1044    Orsi, A. H., Whitworth III, T., and Nowlin Jr, W. D.: On the meridional extent and fronts of the

1045        Antarctic Circumpolar Current, Deep Sea Research Part I: Oceanographic Research Papers, 42,

1046        641-673, 1995.

1047    Otto-Bliesner, B., Brady, E., Zhao, A., Brierley, C., Axford, Y., Capron, E., Govin, A., Hoffman, J.,

1048        Isaacs, E., and Kageyama, M.: Large-scale features of Last Interglacial climate: Results from

1049        evaluating the lig127k simulations for CMIP6-PMIP4, Climate of the Past, 17, 63-94, 2021.

1050    Otto-Bliesner, B. L., Braconnot, P., Harrison, S. P., Lunt, D. J., Abe-Ouchi, A., Albani, S., Bartlein,

1051        P. J., Capron, E., Carlson, A. E., and Dutton, A.: The PMIP4 contribution to CMIP6–Part 2: Two

1052        interglacials, scientific objective and experimental design for Holocene and Last Interglacial

1053        simulations, Geoscientific Model Development, 10, 3979-4003, 2017.

1054    Park, E., Hefter, J., Fischer, G., Iversen, M. H., Ramondenc, S., Nöthig, E.-M., and Mollenhauer,

1055        G.: Seasonality of archaeal lipid flux and GDGT-based thermometry in sinking particles of high-

1056        latitude oceans: Fram Strait (79° N) and Antarctic Polar Front (50° S), Biogeosciences, 16, 2247-

1057        2268, 2019.

1058    Parkinson, C. L., and Cavalieri, D. J.: Antarctic sea ice variability and trends, 1979-2010, The

1059        Cryosphere, 6, 871-880, 2012.

1060    Parkinson, C. L.: A 40-y record reveals gradual Antarctic sea ice increases followed by decreases at

1061        rates far exceeding the rates seen in the Arctic, Proceedings of the National Academy of Sciences,

1062        116, 14414-14423, 2019.

1063    Paul, S., Willmes, S., and Heinemann, G.: Long-term coastal-polynya dynamics in the southern

1064        Weddell Sea from MODIS thermal-infrared imagery, The Cryosphere, 9, 2027-2041, 2015.

1065    Pritchard, H., Ligtenberg, S., Fricker, H., Vaughan, D., Van den Broeke, M., and Padman, L.:

1066        Antarctic ice-sheet loss driven by basal melting of ice shelves, Nature, 484, 502-505, 2012.

1067    Raddatz, T., Reick, C., Knorr, W., Kattge, J., Roeckner, E., Schnur, R., Schnitzler, K.-G., Wetzel,

1068        P., and Jungclaus, J.: Will the tropical land biosphere dominate the climate–carbon cycle

1069        feedback during the twenty-first century?, Climate dynamics, 29, 565-574, 2007.

1070      Riaux-Gobin, C., and Poulin, M.: Possible symbiosis of Berkeleya adeliensis Medlin, Synedropsis

1071          fragilis (Manguin) Hasle et al. and Nitzschia lecointei Van Heurck (Bacillariophyta) associated

1072          with land-fast ice in Adélie Land, Antarctica, Diatom Research, 19, 265-274, 2004.

1073      Riaux-Gobin, C., Dieckmann, G. S., Poulin, M., Neveux, J., Labrune, C., and Vetion, G.:

1074          Environmental conditions, particle flux and sympagic microalgal succession in spring before the

1075          sea-ice break-up in Adélie Land, East Antarctica, Polar Research, 32,

1076          https://doi.org/10.3402/polar.v32i0.19675, 2013.

1077      Rignot, E., Mouginot, J., Scheuchl, B., Van Den Broeke, M., Van Wessem, M.J., Morlighem, M.:

1078          Four decades of Antarctic Ice Sheet mass balance from 1979–2017. Proceedings of the National

1079          Academy of Sciences 116, 1095-1103, 2019.

1080      Rintoul, S., Hughes, C., and Olbers, D.: The Antarctic circumpolar current system, International

1081          Geophysics, 77, 271-302, 2001.

1082      Roeckner, E., Dümenil, L., Kirk, E., Lunkeit, F., Ponater, M., Rockel, B., Sausen, R., and Schlese,

1083          U.: The Hamburg version of the ECMWF model (ECHAM), Research activities in atmospheric

1084          and oceanic modelling. CAS/JSC Working Group on Numerical Experimentation, 13, 7.1-7.4,

1085          1989.

1086      Rontani, J.-F., Smik, L. and Belt, S.T.: Autoxidation of the sea ice biomarker proxy $IPSO_{25}$ in the

1087          near-surface oxic layers of Arctic and Antarctic sediments, Organic Geochemistry 129, 63-76,

1088          2019.

1089      Rontani, J.-F., Belt, S.T. and Amiraux, R.: Biotic and abiotic degradation of the sea ice diatom

1090          biomarker $IP_{25}$ and selected algal sterols in near-surface Arctic sediments, Organic Geochemistry

1091          118, 73-88, 2018.

1092      Sangrà, P., Gordo, C., Hernández-Arencibia, M., Marrero-Díaz, A., Rodríguez-Santana, A., Stegner,

1093          A., Martínez-Marrero, A., Pelegrí, J. L., and Pichon, T.: The Bransfield current system, Deep Sea

1094          Research Part I: Oceanographic Research Papers, 58, 390-402, 2011.

1095      Scambos, T. A., Bell, R. E., Alley, R. B., Anandakrishnan, S., Bromwich, D., Brunt, K.,

1096          Christianson, K., Creyts, T., Das, S., and DeConto, R.: How much, how fast?: A science review

1097     and outlook for research on the instability of Antarctica's Thwaites Glacier in the 21st century,

1098     Global and Planetary Change, 153, 16-34, 2017.

1099 Schmidt, K., Brown, T. A., Belt, S. T., Ireland, L. C., Taylor, K. W., Thorpe, S. E., Ward, P., and

1100     Atkinson, A.: Do pelagic grazers benefit from sea ice? Insights from the Antarctic sea ice proxy

1101     $IPSO_{25}$, 15, 1987-2006, 2018.

1102 Schmidtko, S., Heywood, K. J., Thompson, A. F., and Aoki, S.: Multidecadal warming of Antarctic

1103     waters, Science, 346, 1227-1231, 2014.

1104 Schofield, O., Brown, M., Kohut, J., Nardelli, S., Saba, G., Waite, N., and Ducklow, H.: Changes in

1105     the upper ocean mixed layer and phytoplankton productivity along the West Antarctic Peninsula,

1106     Philosophical Transactions of the Royal Society A: Mathematical, Physical and Engineering

1107     Sciences, 376, https://doi.org/10.1098/rsta.2017.0173, 2018.

1108 Schouten, S., Hopmans, E. C., Schefuß, E., and Sinninghe Damsté, J. S.: Distributional variations in

1109     marine crenarchaeotal membrane lipids: a new tool for reconstructing ancient sea water

1110     temperatures?, Earth and Planetary Science Letters, 204, 265-274, 2002.

1111 Schouten, S., Hopmans, E. C., and Sinninghe Damsté, J. S.: The organic geochemistry of glycerol

1112     dialkyl glycerol tetraether lipids: A review, Organic Geochemistry, 54, 19-61, 2013.

1113 Schröder, M.: The Expedition PS111 of the Research POLARSTERN to the southern Weddell Sea

1114     in 2018, Berichte zur Polar-und Meeresforschung = Reports on polar and marine research, 718,

1115     2018.

1116 Sidorenko, D., Goessling, H., Koldunov, N., Scholz, P., Danilov, S., Barbi, D., Cabos, W., Gurses,

1117     O., Harig, S., and Hinrichs, C.: Evaluation of FESOM2. 0 coupled to ECHAM6. 3: Preindustrial

1118     and HighResMIP simulations, Journal of Advances in Modeling Earth Systems, 11, 3794-3815,

1119     2019.

1120 Smik, L., Belt, S. T., Lieser, J. L., Armand, L. K., and Leventer, A.: Distributions of highly branched

1121     isoprenoid alkenes and other algal lipids in surface waters from East Antarctica: further insights

1122     for biomarker-based paleo sea-ice reconstruction, Organic Geochemistry, 95, 71-80, 2016.

1123 Smith, J.A., Hillenbrand, C.-D., Kuhn, G., Klages, J.P., Graham, A.G.C., Larter, R.D., Ehrmann,

1124     W., Moreton, S.G., Wiers, S., Frederichs, T.: New constraints on the timing of West Antarctic

47

1125     Ice Sheet retreat in the eastern Amundsen Sea since the Last Glacial Maximum. Glob. Planet.

1126     Change 112, 224-237, 2014.

1127 Smith, J.A., Hillenbrand, C.-D., Kuhn, G., Larter, R.D., Graham, A.G.C., Ehrmann, W., Moreton,

1128     S.G., Forwick, M.: Deglacial history of the West Antarctic Ice Sheet in the western Amundsen

1129     Sea Embayment, Quaternary Science Reviews 30, 488-505, 2011.

1130 Smith, J.A., Andersen, T., Shortt, M., Gaffney, A., Truffer, M., Stanton, T.P., Bindschadler, R.,

1131     Dutrieux, P., Jenkins, A., Hillenbrand, C.-D.: Sub-ice-shelf sediments record history of twentieth-

1132     century retreat of Pine Island Glacier, Nature 541, 77-80, 2017.

1133 Spencer-Jones, C. L., McClymont, E. L., Bale, N. J., Hopmans, E. C., Schouten, S., Müller, J.,

1134     Abrahamsen, E. P., Allen, C., Bickert, T., Hillenbrand, C. D., Mawbey, E., Peck, V., Svalova,

1135     A., and Smith, J. A.: Archaeal Intact Polar Lipids in Polar Waters: A Comparison Between the

1136     Amundsen and Scotia Seas, ~~Biogeosciences Discuss. [preprint], https://doi.org/10.5194/bg-2020-~~

1137     ~~333, in review, 2020~~Biogeosciences18, 3485-3504, https://doi.org/10.5194/bg-18-3485-2021,

1138     2021.

1139 Stevens, B., Giorgetta, M., Esch, M., Mauritsen, T., Crueger, T., Rast, S., Salzmann, M., Schmidt,

1140     H., Bader, J., and Block, K.: Atmospheric component of the MPI-M Earth system model:

1141     ECHAM6, Journal of Advances in Modeling Earth Systems, 5, 146-172, 2013.

1142 Stocker, T. F., Qin, D., Plattner, G.-K., Tignor, M., Allen, S. K., Boschung, J., Nauels, A., Xia, Y.,

1143     Bex, V., and Midgley, P. M.: The physical science basis. Contribution of working group I to the

1144     fifth assessment report of the intergovernmental panel on climate change, Computational

1145     Geometry, 18, 95-123, 2013.

1146 Tesi, T., Belt, S., Gariboldi, K., Muschitiello, F., Smik, L., Finocchiaro, F., Giglio, F., Colizza, E.,

1147     Gazzurra, G., and Giordano, P.: Resolving sea ice dynamics in the north-western Ross Sea during

1148     the last 2.6 ka: From seasonal to millennial timescales, Quaternary Science Reviews, 237,

1149     http://dx.doi.org/10.1016/j.quascirev.2020.106299, 2020.

1150 Thomas, D. N.: Sea ice, John Wiley & Sons, 2017.

1151 Thompson, A. F., Heywood, K. J., Thorpe, S. E., Renner, A. H., and Trasviña, A.: Surface circulation
1152     at the tip of the Antarctic Peninsula from drifters, Journal of Physical Oceanography, 39, 3-26,
1153     2009.

1154 Thompson, A. F., Stewart, A. L., Spence, P., and Heywood, K. J.: The Antarctic Slope Current in a
1155     changing climate, Reviews of Geophysics, 56, 741-770, 2018.

1156 Turner, J., Orr, A., Gudmundsson, G. H., Jenkins, A., Bingham, R. G., Hillenbrand, C.-D., and
1157     Bracegirdle, T. J.: Atmosphere-ocean-ice interactions in the Amundsen Sea Embayment, West
1158     Antarctica, Reviews of Geophysics, 55, 235-276, 2017.

1159 Turner, J., Guarino, M.V., Arnatt, J., Jena, B., Marshall, G.J., Phillips, T., Bajish, C.C., Clem, K.,
1160     Wang, Z., Andersson, T., Murphy, E.J., Cavanagh, R.: Recent Decrease of Summer Sea Ice in
1161     the Weddell Sea, Antarctica, Geophysical Research Letters 47, e2020GL087127, 2020.

1162 Valcke, S.: The OASIS3 coupler: A European climate modelling community software, Geoscientific
1163     Model Development, 6, 373-388, 2013.

1164 Vaughan, D. G., Marshall, G. J., Connolley, W. M., Parkinson, C., Mulvaney, R., Hodgson, D. A.,
1165     King, J. C., Pudsey, C. J., and Turner, J.: Recent rapid regional climate warming on the Antarctic
1166     Peninsula, Climatic change, 60, 243-274, 2003.

1167 Vaughan, D. G.: West Antarctic Ice Sheet collapse–the fall and rise of a paradigm, Climatic Change,
1168     91, 65-79, 2008.

1169 Vernet, M., Geibert, W., Hoppema, M., Brown, P. J., Haas, C., Hellmer, H., Jokat, W., Jullion, L.,
1170     Mazloff, M., and Bakker, D.: The Weddell Gyre, Southern Ocean: present knowledge and future
1171     challenges, Reviews of Geophysics, 57, 623-708, 2019.

1172 Volkman, J. K.: Lipid markers for marine organic matter, in: Marine organic matter: Biomarkers,
1173     isotopes and DNA, Springer, 27-70, 2006.

1174 Vorrath, M.-E., Müller, J., Esper, O., Mollenhauer, G., Haas, C., Schefuß, E., and Fahl, K.: Highly
1175     branched isoprenoids for Southern Ocean sea ice reconstructions: a pilot study from the WAP,
1176     Biogeosciences, 16, 2961-2981, 2019.

1177 Vorrath, M.-E., Müller, J., Rebolledo, L., Cárdenas, P., Shi, X., Esper, O., Opel, T., Geibert, W.,
1178     Muñoz, P., and Haas, C.: Sea ice dynamics in the Bransfield Strait, Antarctic Peninsula, during

1179    the past 240 years: a multi-proxy intercomparison study, Climate of the Past, 16, 2459-2483,

1180    2020.

1181    Wang, Z., Turner, J., Wu, Y., Liu, C.: Rapid Decline of Total Antarctic Sea Ice Extent during 2014–

1182    16 Controlled by Wind-Driven Sea Ice Drift. Journal of Climate 32, 5381-5395, 2019.

1183    Witus, A.E., Branecky, C.M., Anderson, J.B., Szczuciński, W., Schroeder, D.M., Blankenship, D.D.,

1184    Jakobsson, M.: Meltwater intensive glacial retreat in polar environments and investigation of

1185    associated sediments: example from Pine Island Bay, West Antarctica, Quaternary Science

1186    Reviews, 85, 99–118, 2014.

1187    Xiao, X., Fahl, K., Müller, J., and Stein, R.: Sea-ice distribution in the modern Arctic Ocean:

1188    Biomarker records from trans-Arctic Ocean surface sediments, Geochimica et Cosmochimica

1189    Acta, 155, 16-29, 2015.

1190    Zamelczyk, K., Rasmussen, T. L., Husum, K., Haflidason, H., de Vernal, A., Ravna, E. K., Hald,

1191    M., and Hillaire-Marcel, C.: Paleoceanographic changes and calcium carbonate dissolution in the

1192    central Fram Strait during the last 20 ka, Quaternary Research, 78, 405-416, 2012.

1193    Zielinski, U., Gersonde, R., Sieger, R., and Fütterer, D.: Quaternary surface water temperature

1194    estimations: Calibration of a diatom transfer function for the Southern Ocean, Paleoceanography

1195    and Paleoclimatology, 13, 365-383, 1998.

1196    Zwally, H. J.: Antarctic sea ice, 1973-1976: Satellite passive-microwave observations, Scientific and

1197    Technical Information Branch, National Aeronautics and Space, 1983.

1198

1199